Vibrio cholerae MARTX toxin multifunctionality silences inflammatory response to toxin-mediated cytoskeletal collapse

Patrick J. Woida[1], Karla J. F. Satchell[1,2*]

[1]Department of Microbiology-Immunology, Northwestern University Feinberg School of Medicine, Chicago, IL 60611, USA

[2]Corresponding author

*Correspondence. Email k-satchell@northwestern.edu

ABSTRACT

Multifunctional autoprocessing repeats-in-toxin (MARTX) toxins are pore-forming toxins that translocate multiple functionally independent effector domains into a target eukaryotic cell. *Vibrio cholerae* colonizes intestinal epithelial cells (IECs) and utilizes a MARTX toxin with three effector domains — the actin cross-linking domain (ACD), the Rho inactivation domain (RID), and the α/β hydrolase domain (ABH) — to regulate innate immunity and enhance colonization. Whether these multiple catalytic enzymes delivered from a single toxin have coordinated function has not been explored. Using cultured IECs, we demonstrate ACD-induced cytoskeletal collapse activates a robust proinflammatory response that is blocked by the action of co-delivered RID and ABH. Thus, MARTX toxins utilize multiple enzymatic activities on a single toxin to silence the host response to both bacterial factors and effector function. Further, these data explain that *V. cholerae* utilizes the MARTX toxin to suppress intestinal inflammation and contribute to cholera being classically defined as non-inflammatory diarrheal disease.

Keywords: *Vibrio cholerae*, MARTX toxin, interleukin-8, CXCL8, RNA-seq, MAP kinases, signaling

29 **GRAPHICAL ABSTRACT**
30
31

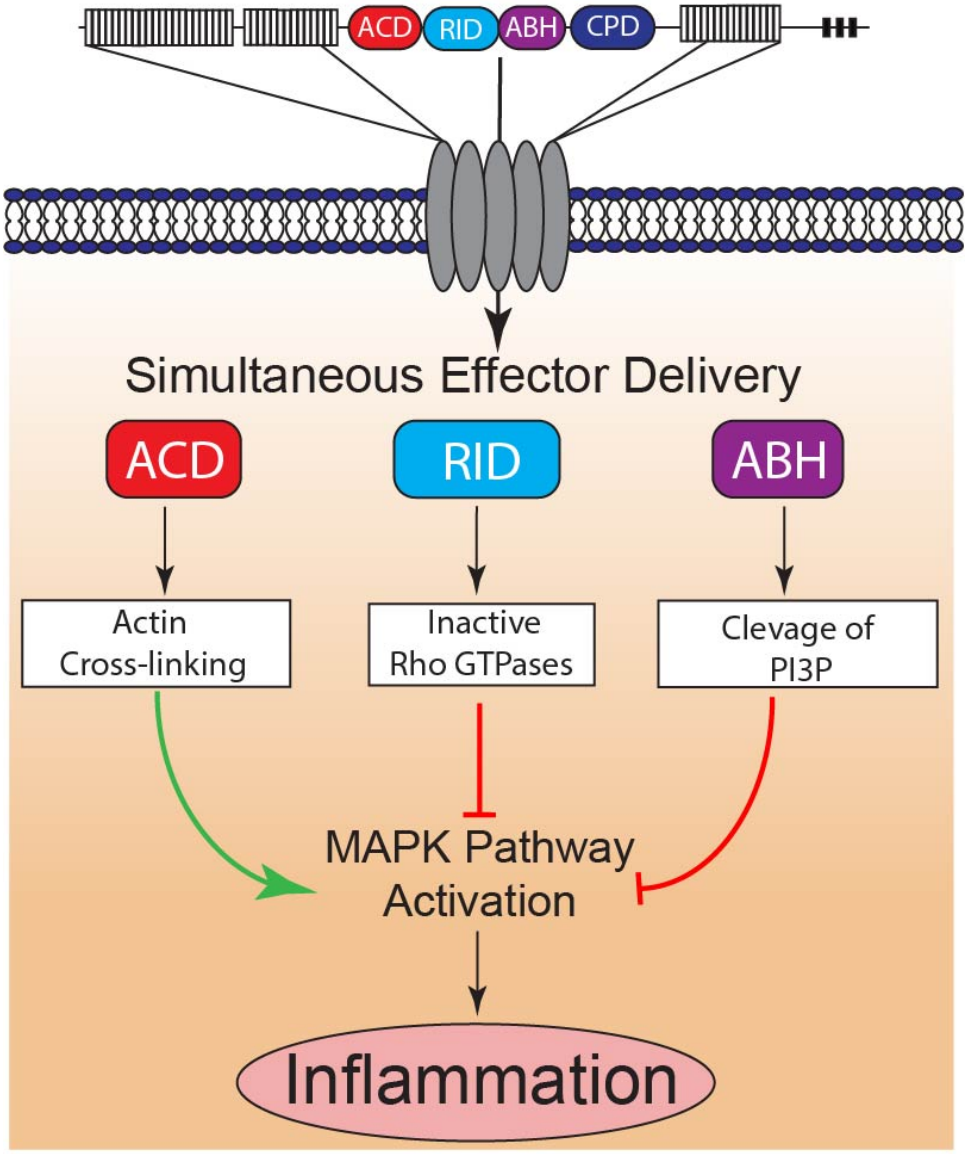

32

INTRODUCTION

Multifunctional autoprocessing repeats-in-toxin (MARTX) toxins utilize multiple enzymatic functions to promote virulence of various *Vibrio* species. MARTX toxins are secreted as single 3500 – 5300 amino acid polypeptides that contain conserved glycine-rich repeats at the N- and C-termini that flank multiple arrayed effector domains and an autoprocessing cysteine protease domain (CPD) (Satchell, 2015). The glycine-rich repeats are proposed to form a pore in the plasma membrane of eukaryotic cells to translocate the arrayed effectors and the CPD into the target cell (Dolores et al., 2015; Kim et al., 2015; Kim et al., 2008). In the cytoplasm, CPD is activated by binding host inositol hexakisphosphate ($InsP_6$) and then auto-cleaves to free the effector domains from the large holotoxin. The individual effectors then can traffic through the cell to identify targets and to perform their catalytic functions (Egerer and Satchell, 2010; Prochazkova et al., 2009; Shen et al., 2009) (Figure 1A). Due to this enzymatic multifunctionality, MARTX toxins have been described as bacterial “cluster bombs” that release multiple cytotoxic bomblets into host cells from a single toxin warhead. While the biochemical function of many of the effector domains is known (Kim, 2018), the additive or synergistic benefit of having all these enzymatic functions delivered on a single toxin has yet to be identified (Woida and Satchell, 2018).

Vibrio cholerae is the causative agent of the severe diarrheal disease cholera (Ali et al., 2012). In addition to its primary virulence factor, the ADP-ribosylating cholera toxin, pandemic *V. cholerae* El Tor O1 strains secrete a 4,545 amino acid (a.a) $MARTX_{Vc}$ toxin that contributes to enhanced bacterial colonization of the small intestine by protecting the pathogen from neutrophil-mediated clearance during the earliest stages of infection (Olivier et al., 2007; Olivier et al., 2009; Queen and Satchell, 2012; Weill et al., 2017). The early timing of these events suggests the inhibition of neutrophils and other innate immune cells does not reflect destruction of the cells by the $MARTX_{Vc}$ toxin, but rather a failure of neutrophils to be recruited to the site of

59 infection. Therefore, the MARTX$_{Vc}$ toxin might function to limit host signaling that results in
60 innate immune cell recruitment.

61 Although MARTX toxins can have highly variable effector domain organizations in some
62 species, the MARTX$_{Vc}$ toxin of nearly all *V. cholerae* strains have the same three effector
63 domains (Dolores and Satchell, 2013) (Figure 1A). The first effector domain is the actin cross-
64 linking domain (ACD) that covalently cross-links monomeric actin to depolymerize actin (Fullner
65 and Mekalanos, 2000; Kudryashov et al., 2008; Sheahan et al., 2004). The cross-linked actin
66 oligomers also have high binding affinity for formins and other actin binding proteins to further
67 disrupt the cytoskeleton (Heisler et al., 2015). The second domain is the Rho inactivation
68 domain (RID) that inactivates Rac1 and other Rho family GTPases by transferring fatty acids
69 onto lysine residues in the C-terminal polybasic region of the GTPases. The acylation of the
70 Rho GTPases blocks them from interacting with downstream effectors. The action of both ACD
71 and RID results in destruction of the actin cytoskeleton and loss of epithelial cell junction
72 integrity (Dolores et al., 2015; Sheahan and Satchell, 2007; Zhou et al., 2017). The final effector
73 domain is the α/β hydrolase domain (ABH), a highly specific phospholipase A1 that cleaves only
74 phosphatidylinositol 3-phosphate (PI3P) to inhibit autophagy and endocytic trafficking in HeLa
75 cells (Agarwal et al., 2015). All three effector domains can also independently disable
76 macrophages, suggesting a mechanism by which the MARTX$_{Vc}$ toxin protects against clearance
77 of *V. cholerae* from the intestine. However, while ACD potently inhibits phagocytosis, inhibition
78 by RID and ABH is far less robust (Dolores et al., 2015). Therefore, in the context of co-
79 introduction into cells in parallel with ACD, phagocytosis is not likely a biologically significant
80 outcome of RID and ABH intoxication. Further, since the MARTX$_{Vc}$ toxin promotes colonization
81 possibly even well before onset of inflammation, inhibition of phagocytic clearance may not be a
82 primary function of the MARTX$_{Vc}$ toxin.

83 Intestinal epithelial cells (IECs) act as a barrier to contain bacteria to the lumen, and also
84 as sensors to detect microbial-associated molecular patterns and release chemokines that

recruit immune cells to the site of infection (Kagnoff and Eckmann, 1997; Peterson and Artis, 2014). While *V. cholerae* is typically considered a secretory, non-inflammatory diarrheal disease, these bacteria do elicit mild inflammation in human intestines (Bishop et al., 2014; Qadri et al., 2002). In addition, *V. cholerae* is known to stimulate release of the neutrophil-recruiting chemokine interleukin-8 (IL-8 or CXCL8) from human colonic intestinal cells in response to pathogen-associated molecular patterns (PAMPs) including purified flagellin and lipopolysaccharide (LPS) (Harrison et al., 2008; Rodriguez et al., 2001; Soriani et al., 2002; Zhou et al., 2004). However, the extent to which *V. cholerae* induces IL-8 secretion *in vitro* in response to live bacteria varies dramatically based on the strain isolate (Rodriguez et al., 2001; Zhou et al., 2004). Since *V. cholerae* routinely induces inflammation in response to purified PAMPs, we hypothesized that the variable response to live bacteria may be attributed to strain-dependent variation in secreted exotoxins impacting initiation of proinflammatory signaling in IECs.

In this study, we show that *V. cholerae* globally suppresses proinflammatory gene expression in IECs and this signaling inhibition is mediated by the catalytic action of the secreted $MARTX_{Vc}$ toxin, and not by other accessory toxins. These results explain observed differences in the inflammatory response to various *V. cholerae* strains and why infections with $MARTX_{Vc}^{+}$ *V. cholerae* induces a highly secretory, but non-inflammatory, diarrhea. Further, we find that the cytoskeletal destruction initiated by the ACD conversely functions as a damage-associated molecular pattern (DAMP) to potently induce proinflammatory gene expression through the mitogen-activated protein kinase (MAPK) pathway; and, this response is more robust even than that induced by bacterial PAMPs. However, in the context of the $MARTX_{Vc}$ holotoxin, co-delivery on the same toxin of RID and ABH silences pathways that would normally transduce the signals to induce proinflammatory gene expression in response to both DAMPs and PAMPs. These data reveal that simultaneous delivery of all three effector domains on a single multifunctional toxin is advantageous as it promotes the ACD-mediated destruction of the

111 actin cytoskeleton without detection of the associated damage by the infected host. Thus,
112 multifunctional toxins can coordinate their multiple enzymatic activities to fine-tune the host
113 response to infection.
114
115 **RESULTS**
116
117 **The MARTX$_{Vc}$, and not HlyA or HapA, inhibits IL-8 secretion from IECs**
118 *V. cholerae* secretes three accessory toxins in addition to cholera toxin: the MARTX$_{Vc}$ toxin
119 encoded by the gene *rtxA*, α-hemolysin encoded by *hlyA*, and hemagglutinin/protease encoded
120 by *hapA*. To evaluate whether accessory toxins modulate IL-8 secretion in IECs, cultured IECs
121 were treated with live *V. cholerae* strain N16961 or previously generated derivatives with
122 deletions in *rtxA*, *hlyA*, or *hapA* (Fullner et al., 2002). N16961 stimulated IL-8 secretion at
123 concentrations similar to untreated control cells (Figure 1B), while N16961Δ*rtxA* induced
124 significantly more IL-8 secretion (Figure 1B). No difference was observed due to loss of HlyA or
125 HapA, or both toxins (*ΔhlyAΔhapA*, heretofor referred to as KFV119) (Figure 1B). These results
126 reveal that N16961 has the potential to stimulate release of IL-8 from IECs, but the MARTX$_{Vc}$
127 toxin actively suppresses the response.
128 The atypical El Tor O1 strain 2010EL-1786 from the 2010 Haiti outbreak is known to be
129 more proinflammatory (Satchell et al., 2016). This strain has a premature stop codon in *rtxA* that
130 prevents secretion of the MARTX$_{Vc}$ toxin (Dolores and Satchell, 2013). Consistent with results
131 using N16961, 2010EL-1786 induced a significant increase in IL-8 secretion from IECs, but this
132 response was suppressed when the stop codon in *rtxA* was restored to a Trp codon (Figure
133 1C). These results show that *V. cholerae* activates proinflammatory chemokine secretion, but
134 this is suppressed in *rtxA*$^{+}$ *V. cholerae* strains.
135

MARTX$_{Vc}$ toxin effector domains, and not the pore, inhibit IL-8 secretion in IECs

The MARTX$_{Vc}$ toxin has four putative cytotoxic functions, the formation of a pore and the biochemical activities of its three effector domains (Woida and Satchell, 2018). In previous studies (Dolores et al., 2015), a derivative of KFV119 was generated in which the *rtxA* gene was modified to replace sequences that encode the effector domains with an in-frame sequence for β-lactamase (Bla). This strain produces a toxin that forms a functional pore and is able to translocate, but lacks all effector activity (*rtxA::bla*). The individual effector domains ACD (*acd::bla*), RID (*rid::bla*), and ABH (*abh::bla*) were then individually restored into the parent *rtxA::bla* strain to create effector gain of function toxins (Figure 2A-E). Catalytically inactive effector derivatives of these toxins and a Δ*rtx* negative control strain were also generated and characterized.

The *rtxA::bla* strain induced similar levels of IL-8 secretion from intestinal cells as the *Δrtx* strain, but significantly higher than KFV119 (Figure 2F). This result indicates that the MARTX$_{Vc}$ pore alone does not suppress IL-8 secretion. Surprisingly, the *acd::bla* strain induced significantly more IL-8 secretion compared to both the *Δrtx* and *rtxA::bla* strains (Figure 2F). The *rid::bla* strain induced IL-8 secretion equivalent to KFV119 (Figure 2F). These results indicate that RID is sufficient to suppress *V. cholerae*-induced IL-8 secretion, while ACD actually exacerbates IL-8 secretion beyond stimulation by live bacteria. The *abh::bla* strain had no effect on *V. cholerae*-induced IL-8 secretion (Figure 2F). In fact, when intestinal cells were simultaneously co-inoculated with both the *acd::bla* and the *rid::bla* strains, IL-8 secretion was also suppressed (Figure 2G). This was due to the acylation activity of RID, since the *rid*-H2782A*::bla* catalytically inactive strain did not suppress IL-8. In addition, although less robust, co-inoculation of *acd::bla* with *abh::bla* also attenuated IL-8 secretion (Figure 2G). These results reveal that RID, and to a lesser extent ABH, inhibits both bacterial- and ACD-induced IL-8 secretion.

161

162 **The MARTX$_{Vc}$ toxin inhibits expression of the *CXCL8* gene**

163 A block to IL-8 secretion can occur by inhibition of IL-8 protein secretion or inhibition of
164 IL-8 (*CXCL8*) gene expression. At two hours post-inoculation, there was no significant change in
165 transcription of the *CXCL8* gene in intestinal cells inoculated with KFV119 or *Δrtx* compared to
166 mock-treated cells (Figure 2H). There was also no significant change due to RID or ABH. By
167 contrast, a significant 32-fold increase was induced by ACD (Figure 2H). These results indicate
168 that MARTX$_{Vc}$ effector domain modulation of IL-8 secretion occurred primarily due to blocking of
169 *CXCL8* gene transcription.

170 The absence of a response to *Δrtx* was unexpected since *V. cholerae* alone induced IL-8
171 secretion (Figure 1B, 2F) (Zhou et al., 2004). Since chemokine secretion from cells by ELISA
172 requires a long incubation period following bacterial challenge, we hypothesized that the IEC
173 response to *V. cholerae* occurs after the 120 minutes (min) bacterial challenge in which *CXCL8*
174 expression was assayed. Therefore, changes in *CXCL8* expression were measured overtime
175 following bacterial challenge. Confirming previous results, no change in *CXCL8* expression was
176 observed by KFV119 at any timepoint measured (Figure 2I). However, while *Δrtx* did not induce
177 changes in expression at 120 min post-inoculation, there was a significant 10-fold increase in
178 expression at six hours post-inoculation that eventually returned to baseline between 12 and 22
179 hours (Figure 2I). As observed previously, *acd::bla* induced a significant 42-fold change in
180 *CXCL8* expression at two hours. While this response diminished overtime, *CXCL8* mRNA levels
181 remained 10- to 18-fold higher than mock-treated cells (Figure 2I). These data further show that
182 ACD-mediated *CXCL8* expression is stimulated as much as four hours before *V. cholerae*-
183 induced gene expression. Therefore, in addition to suppressing the host response to effector
184 activity, *V. cholerae* may utilize the MARTX$_{Vc}$ toxin to disable host inflammatory responses prior

185 to detection of bacterial PAMPs, such as flagellin and LPS (Harrison et al., 2008; Soriani et al.,
186 2002).
187
188 **ACD, but not the MARTX$_{Vc}$ holotoxin, induces proinflammatory gene expression in IECs**
189 To determine the breadth of the proinflammatory immune response stimulated by ACD, we
190 utilized a whole transcriptome RNA-sequencing (RNA-seq) approach. Cell were treated with
191 various bacterial strains for two hours prior to transcriptional profiling. Statistically significant
192 results were given a $-1 \leq 0 \leq 1$ $\log_2$ fold change cut off to adjust for biologically significant
193 changes (Figure 3A-B). A single gene *JUN* was upregulated by KFV119 compared to
194 uninoculated cells, but this upregulation was not consistent when validated by qPCR (Figure
195 3C). Thus, there was no significant upregulation of any host gene after two hours treatment of
196 IECs with MARTX$_{Vc}$+ *V. cholerae*.
197 Similarly, *rid::bla, abh::bla,* and *Δrtx* also did not induce significant changes in IEC gene
198 expression by two hours. By contrast, the *acd::bla* strain induced differential regulation of over
199 200 genes. Many of the significantly upregulated genes by ACD were identified as regulators of
200 inflammation. These include genes for chemokines CXCL8 (IL-8) and CXCL3 (IL-3), cytokine
201 TNF, and for proinflammatory transcription factors JUN, FOS, and EGR1/2/3 (Fig 3B-G).
202 Upregulation of select proinflammatory genes was validated by qPCR (Figure 2H, 3C-G). These
203 data suggest that when delivered independently, ACD induces proinflammatory gene
204 expression more rapidly than by *V. cholerae* alone. However, when ACD is delivered on the
205 complete MARTX$_{Vc}$ toxin, the response is abolished.
206
207 **RID and ABH suppress host MAPK signaling to modulate the ACD proinflammatory**
208 **response**

209 Bioinformatic analysis of the *acd::bla* differentially regulated genes revealed that many
210 were associated with the ERK, p38, JNK MAPK and NF-κB pathways (Figure 3H). These
211 pathways have also been associated with induction of IL-8 by purified *V. cholerae* flagellin
212 (Harrison et al., 2008). The phosphorylation of MAPK in bacterial-treated cells was monitored
213 after two hours. While KFV119-treated cells showed no ERK phosphorylation, *Δrtx* activated
214 ERK signaling (Figure 3I). Further, *acd::bla* stimulated phospho-ERK levels above that of *Δrtx*
215 alone (Figure 3I). Both the *rid::bla* and *abh::bla* strains suppressed phospho-ERK, while *rid*-
216 H2782A*::bla* and *abh*-H3369A::*bla* strains did not (Figure 3I). KFV119-treated cells also showed
217 no phosphorylation of p38 or JNK. However, these MAPK pathways were activated by *acd::bla*
218 (Figure 3J and K). While previous studies suggest *V. cholerae* PAMPs may also activate these
219 pathways (Harrison et al., 2008), the observed limited or undetectable p38 and JNK MAPK
220 phosphorylation by *Δrtx* alone is likely a result of timing, since *V. cholerae* does not induce
221 expression of proinflammatory genes until six hours post-inoculation (Figure 2I and 3A). Finally,
222 none of the effector domains inhibited NF-κB, as measured by IκBα degradation (Figure 3L).
223 The lack of MAPK activation in $MARTX_{Vc}^{+}$ KFV119-treated cells suggests there is active
224 suppression of ACD-induced MAPK signaling due to interplay between the $MARTX_{Vc}$ effector
225 domains. However, these experiments rely on comparing strains with only one effector to those
226 with either all or no effectors. To study interactions between effector domains requires $MARTX_{Vc}$
227 toxin strains that simultaneously deliver two active effectors into a cell on a single toxin. Six new
228 strains with introduced codon changes in *rtxA* were generated to produce $MARTX_{Vc}$ toxins that
229 retain natural processing and delivery of all effectors, but with one, two, or all three of the
230 effectors carrying point mutations in essential catalytic site residues (Figure 4A and Figure S1).
231 Cells treated with these strains confirmed results above that ACD-induced IL-8 secretion is
232 suppressed by both RID and ABH (Figure 4B). However, unlike *abh:bla*, the ABH Active Only

strain also significantly reduced bacterial secretion of IL-8 (Figure 4B). Therefore, when delivered on the complete holotoxin, ABH can suppress *V. cholerae* induction of IL-8.

To determine if both RID and ABH can suppress ACD upregulation of MAPK signaling, activation of these pathways were examined in cells treated with the newly constructed strains. The single active ACD strain stimulated ERK activation beyond that of *V. cholerae* alone, while both the single active RID and ABH strains suppressed bacterial activation of ERK (Figure 4C). Additionally, both the Active ACD/RID and Active ACD/ABH strain showed attenuation of ACD-induced phospho-ERK, phospho-JNK and phospho-p38 compared to the ACD Active only strain (Figure 4C-E).

Further, cells treated with PD98059, an inhibitor of ERK, showed no attenuation of the IL-8 response (Figure 4F). However, inhibition of the p38 MAPK pathway by SB202190 did inhibit IL-8 secretion (Figure 4G), while inhibition of the JNK pathway by SP600125 had no effect on IL-8 secretion (Figure 4H).

In total, these data show that suppression of MAPK signaling pathways, particularly the p38 pathway, can modulate the ACD-induced proinflammatory response, and this response is attenuated by the action of RID and ABH.

Cytoskeletal collapse can activate proinflammatory signaling in ACD-treated cells, but the signaling is not detected due to prior action of RID and ABH

ACD has two putative cytotoxic functions. The first is the inhibitor action of toxic actin oligomers (dimers and trimers) formed when only 2-4% of total actin has been cross-linked (Heisler et al., 2015; Kudryashova et al., 2018). The second is ACD will eventually cross-link nearly 100% of cellular actin into higher order oligomers (10 to 15-mers) to sequester bulk actin and induce cytoskeletal collapse (Fullner and Mekalanos, 2000). Kinetic experiments comparing actin cross-linking abundance to MAPK activation were performed to determine which of these functions activate MAPK signaling. The ACD Active Only strain induced a maximum of 4% of

total actin cross-linked between 5 and 15 min after addition of *V. cholerae*, corresponding to the formation of early toxic actin oligomers (Figures 5A-B and S2). Cross-linking increased around 60 min (Figure 5A-B) corresponded to ACD sequestering bulk actin to induce actin depolymerization and cytoskeletal collapse. In the same assayed samples, MAPK signaling was activated between 60 and 90 min (Figure 5C-H), when over 50% total monomeric actin was cross-linked. These results indicate that a significant portion of actin needs to be cross-linked to activate proinflammatory signaling. While the Triple* strain showed stochastic activation of MAPK signaling between 5 and 15 min, it induced significantly less ERK phosphorylation than the ACD Active Only strain and there was no detection of phospho-p38 or phospho-JNK between 30 and 120 min (Figure S3C-H). These data suggest that it is ACD sequestration of bulk actin and cytoskeletal destruction that leads to activation of proinflammatory signaling in IECs.

To completely block the intestinal inflammatory response, RID and ABH would have to inactivate MAPK signaling prior to host detection of ACD-induced cytoskeletal collapse. This would indicate that instead of reversing the activation state of MAPK pathways after 60-90 min, RID and ABH inactive these pathways ahead of ACD-induced activation. Cells treated with KFV119 failed to induce any changes in MAPK activation following significant actin cross-linking (Figure 6A-F). Further, both the ACD/RID Active strain and the ACD/ABH Active strain showed reduced phosphorylation of ERK, p38, and JNK, even following significant actin cross-linking at 60 min (Figure S4A-L). Additionally, MAPK activation induced by the Active ACD/RID and Active ACD/ABH strains was still significantly less than activation by the ACD Active only strain at 120 min (Figure 6D-F). These data would suggest that RID and ABH are each sufficient to attenuate ACD induction of MAPK signaling. However, modest, yet significant, activation of the JNK pathway by the Active ACD/RID strain was still observed at 120 min (Figure S4A-F). The Active ACD/ABH strain also induced slight, yet significant, activation of the p38 and JNK pathways at 120 min (Figure S4G-L). Since both RID and ABH alone do not completely abolish activation of

these pathways, both effectors may be required to completely abolish the global inflammatory response observed in the RNA-seq analysis (Figure 3A). The inhibition of MAPK signaling was not due to RID and ABH directly inhibiting ACD actin cross-linking activity. In fact, the ACD/ABH strain showed slight, yet significant, increase in actin cross-linking at 30 and 60 min before returning to similar abundances at 90 and 120 min (Figure S4M). Therefore, both RID and ABH independently silence signal transduction pathways prior to host detection of ACD induced collapse of the actin cytoskeleton without modulating ACD activity.

RID can inhibit IL-8 secretion due to actin destruction by ACD and by latrunculin A, independent of live bacteria or formin inhibition.

To determine if the action of RID is specific to MARTX toxins or more broadly applicable, cells were treated with purified recombinant ACD fused to the N-terminal of the anthrax lethal toxin (LF_NACD) in combination with the anthrax protective antigen (PA). This previously characterized system allows for the delivery of MARTX effector domains into cells in the absence of bacteria and MARTX toxin delivery (Figure 7A) (Cordero et al., 2006). Only cells treated with LF_NACD and PA induced IL-8 secretion, demonstrating that ACD is sufficient for induction of a proinflammatory immune response in the absence of a bacterium. This response was inhibited by co-treating cells with both LF_NACD and LF_NRID in the presence of PA (Figure 7B). Chemical depolymerization of actin also can induce IL-8 secretion (Bobo et al., 2013). Indeed, cells treated with latrunculin A, a sponge toxin that binds and sequesters G-actin, also showed IL-8 secretion. Showing that the mechanisms are conserved, treatment of cells with LF_NRID in the presence of PA suppressed latrunculin A induced IL-8 secretion (Figure 7C). However, inhibiting formins with SMIFH2 failed to elicit an IL-8 response (Figure 7D). These data support that cytoskeletal collapse stimulates the inflammatory pathways and, regardless of the inducer, these pathways are inhibited by RID.

DISCUSSION

MARTX toxins are unique hybrids of independently secreted toxins and multifunctional effector delivery systems (Gavin and Satchell, 2015; Kim, 2018). This study demonstrates that the *V. cholerae* MARTX toxin utilizes this multifunctionality to "self-regulate" and silence the host response both to its own cytotoxic activity and detection of bacterial PAMPs. Following translocation, ACD begins cross-linking actin to produce early toxic oligomers that sequester actin binding proteins and disrupt intestinal tight junctions. While these toxic oligomers are being formed, RID and ABH block MAPK signaling. Once ACD begins to sequester bulk actin to induce cytoskeletal collapse, the cell is unable to trigger MAPK activation. Therefore, the $MARTX_{Vc}$ toxin blocks IECs from activating an innate immune response (Figure 7E). While previous studies have suggested $MARTX^{+}$ *V. cholerae* strains induce IL-8 secretion, those studies found this proinflammatory response to be growth phase dependent in which stationary phase cultures contain more IL-8 than log phase cultures (Zhou et al., 2004). Secretion of the $MARTX_{Vc}$ toxin is also growth phase dependent and is expressed and secreted during log phase and then toxin present in the supernatant fluids is degraded by proteases during stationary phase (Boardman et al., 2007). Therefore, no toxin would be present to suppress IL-8 secretion. Our findings support a new model in which $MARTX_{Vc}$ toxin produced during the early active growth stage in the intestines acts to suppress the IEC inflammatory response. These data indicate that $MARTX_{Vc}$ toxin suppression of intestinal innate immunity prevents host recruitment of immune cells to protect the bacteria from neutrophil-mediated clearance. Additionally, $MARTX_{Vc}$ toxin immunomodulatory activities may contribute to the differences in inflammation observed between various *V. cholerae* strains (Rodriguez et al., 2001; Zhou et al., 2004).

The current predominant circulating *V. cholerae* strains responsible for disease are altered El Tor isolate that are hypervirulent and exhibit increased clinical severity of diarrhea

(Alam et al., 2011; Son et al., 2011). This is in part due to the acquisition of mutations in H-NS and VieA resulting in increased production of cholera toxin and HlyA, increased motility, and inflammasome activation suggesting increased inflammation (Russell et al., 2018; Satchell et al., 2016; Son et al., 2011). In addition, these strains naturally lack the $MARTX_{Vc}$ toxin due to a stop codon in *rtxA*. Restoring toxin secretion in altered El Tor isolate 2010EL-1786 attenuated IL-8 induction comparable to the parent strain (Figure 1C). Thus, loss of the $MARTX_{Vc}$ toxin immunomodulatory activities in these altered strains may increase intestinal inflammation, which could exacerbate disease severity and contribute to its hypervirulence.

The effector domains, and not the $MARTX_{Vc}$ pore, were identified to modulate innate immune signaling in IECs (Figure 2, 4). These data support a previously established model in which the MARTX pore functions primarily as an effector delivery platform and not a direct virulence mechanism (Gavin et al., 2017). How each delivered effector contributes to pathogenesis is still debated. While other studies have connected RID and ABH to inhibition of macrophage phagocytosis *in vitro* (Chen et al., 2017; Zhou et al., 2017), these conclusions contradicted previous findings that 5% inhibition by these effectors is biologically insignificant compared to the 90% inhibition by ACD (Dolores et al., 2015). Our study validates that RID and ABH most likely function primarily to abolish host detection of cytoskeletal damage and bacterial PAMPs. RID-mediated inactivation of MAPK pathways most likely occurs through its direct inactivation of Rho family GTPases. Rho GTPases regulate MAPK and other cell signaling pathways and bacterial toxin inactivation of Rho GTPase can inhibit these pathways in specific cell types (Schwartz, 2004; Woolery et al., 2014). However, toxin inactivation of Rho GTPases through covalent modifications, such as ampylation or glycosylation, induces IL-8 secretion in IECs and activates the pyrin inflammasome in macrophages (Mahida et al., 1996; Xu et al., 2014). However, RID does not activate the inflammasome (Xu et al., 2014). Therefore, RID acylation of the C-terminal polybasic region of Rho family GTPases allows for the inactivation of

362 Rho GTPases to suppress proinflammatory signaling pathways in IECs, while also evading host
363 detection of Rho inactivation through the inflammasome.

364 How cleavage of PI3P by ABH blocks proinflammatory pathways is still unknown. PI3P
365 is required for the formation of autophagosomes and ABH-mediated cleavage of PI3P inhibits
366 formation of autophagosomes and endocytic trafficking (Agarwal et al., 2015). We postulate that
367 ABH depletion of PI3P could block formation of scaffolding complexes on autophagosomes and
368 endosomes that promote recruitment and activation of MAPK signaling molecules
369 (Fehrenbacher et al., 2009; Martinez-Lopez et al., 2013). The loss of the scaffolds would then
370 prevent activation of the MAPK pathway.

371 ACD production of toxic actin oligomers was recently characterized as the primary
372 cytotoxic mechanism of ACD based on the hypothesis that the kinetics of ACD actin cross-
373 linking prevent it from cross-linking the majority of cellular actin (Heisler et al., 2015). Our study
374 reveals ACD stimulation of MAPK signaling pathways occur following cross-linking of over 50%
375 of cellular actin (Figure 6, 7). This supports previous findings in which type VI secreted ACD
376 cross-links significant quantities of actin and induce intestinal inflammation mice (Ma and
377 Mekalanos, 2010). While the toxic oligomers may still contribute to cytoskeletal collapse, our
378 data indicate that it is the destruction of the cytoskeleton, and not the direct formation of toxic
379 actin oligomers inhibition of formins, that activate proinflammatory signaling.

380 RID and ABH silencing the global response to ACD activity provide evidence that
381 different MARTX effector domain combinations could impact the overall host response to co-
382 delivered effectors. These data suggest that an effector's contribution to virulence and disease
383 could be enhanced or attenuated depending on which other effector domains it is delivered with.
384 *V. vulnificus* with different natural effector combinations have varying virulence potential and
385 promote altered host responses (Gavin and Satchell, 2018; Kwak et al., 2011; Murciano et al.,
386 2017). Therefore, MARTX toxin multifunctionality, in combination with variability in the effector

387 domain repertoire, allows for variety of effector interplay combinations which could either
388 enhance or attenuate MARTX toxin associated virulence.
389
390 **ACKNOWLEDGEMENTS**
391 We would like to thank the Northwestern University Center for Genetic Medicine NUSeq core
392 facility, especially Xinkun Wang and Matthew Schipma, for technical assistance, bioinformatic
393 analysis of the RNA-sequencing experiments and DNA sequencing. We would like to thank
394 members of the Satchell lab for their valuable input and technical support and Dr. Nicholas
395 Cianciotto and Dr. Gail Hecht for review of the manuscript. This work was supported by the NIH
396 Ruth L. Kirschstein Institutional National Research Service Award Training Grant in Immunology
397 and Microbial Pathogenesis T32AI007476 (to P.J.W.) and NIH grants R01AI092825 and
398 R01AI098369 (to K.J.F.S.).
399
400 **AUTHOR CONTRIBUTIONS**
401 P.J.W. conceptualized, designed, and conducted all experiments. K.J.F.S advised on all
402 experiments. P.J.W. wrote the original draft of the manuscript and both P.J.W. and K.J.F.S.
403 reviewed and edited the manuscript.
404
405 **CONFLICT OF INTEREST**
406 The authors declare no conflict of interest.
407
408 **REFERENCES**
409 Agarwal, S., Kim, H., Chan, R.B., Agarwal, S., Williamson, R., Cho, W., Paolo, G.D., and
410 Satchell, K.J. (2015). Autophagy and endosomal trafficking inhibition by *Vibrio cholerae* MARTX
411 toxin phosphatidylinositol-3-phosphate-specific phospholipase A1 activity. Nat Commun. *6*,
412 8745.

413 Ahrens, S., Geissler, B., and Satchell, K.J. (2013). Identification of a His-Asp-Cys catalytic triad
414 essential for function of the Rho inactivation domain (RID) of *Vibrio cholerae* MARTX toxin. J
415 Biol Chem. *288*, 1397-1408.
416 Alam, M., Islam, A., Bhuiyan, N.A., Rahim, N., Hossain, A., Khan, G.Y., Ahmed, D., Watanabe,
417 H., Izumiya, H., Faruque, A.S., et al. (2011). Clonal transmission, dual peak, and off-season
418 cholera in Bangladesh. Infect Ecol Epidemiol. *1*.
419 Ali, M., Lopez, A.L., You, Y.A., Kim, Y.E., Sah, B., Maskery, B., and Clemens, J. (2012). The
420 global burden of cholera. Bull World Health Organ. *90*, 209-218A.
421 Anders, S., Pyl, P.T., and Huber, W. (2015). HTSeq--a Python framework to work with high-
422 throughput sequencing data. Bioinformatics. *31*, 166-169.
423 Bishop, A.L., Patimalla, B., and Camilli, A. (2014). *Vibrio cholerae*-induced inflammation in the
424 neonatal mouse cholera model. Infect Immun. *82*, 2434-2447.
425 Boardman, B.K., Meehan, B.M., and Fullner Satchell, K.J. (2007). Growth phase regulation of
426 *Vibrio cholerae* RTX toxin export. J Bacteriol. *189*, 1827-1835.
427 Bobo, L.D., El Feghaly, R.E., Chen, Y.S., Dubberke, E.R., Han, Z., Baker, A.H., Li, J., Burnham,
428 C.A., and Haslam, D.B. (2013). MAPK-activated protein kinase 2 contributes to Clostridium
429 difficile-associated inflammation. Infect Immun. *81*, 713-722.
430 Carmona-Saez, P., Chagoyen, M., Tirado, F., Carazo, J.M., and Pascual-Montano, A. (2007).
431 GENECODIS: a web-based tool for finding significant concurrent annotations in gene lists.
432 Genome Biol. *8*, R3.
433 Chen, C.L., Chien, S.C., Leu, T.H., Harn, H.I., Tang, M.J., and Hor, L.I. (2017). *Vibrio vulnificus*
434 MARTX cytotoxin causes inactivation of phagocytosis-related signaling molecules in
435 macrophages. J Biomed Sci. *24*, 58.
436 Cordero, C.L., Kudryashov, D.S., Reisler, E., and Satchell, K.J. (2006). The Actin cross-linking
437 domain of the *Vibrio cholerae* RTX toxin directly catalyzes the covalent cross-linking of actin. J
438 Biol Chem. *281*, 32366-32374.

Dobin, A., Davis, C.A., Schlesinger, F., Drenkow, J., Zaleski, C., Jha, S., Batut, P., Chaisson, M., and Gingeras, T.R. (2013). STAR: ultrafast universal RNA-seq aligner. Bioinformatics. *29*, 15-21.

Dolores, J., and Satchell, K.J. (2013). Analysis of *Vibrio cholerae* genome sequences reveals unique rtxA variants in environmental strains and an rtxA-null mutation in recent altered El Tor isolates. MBio. *4*, e00624.

Dolores, J.S., Agarwal, S., Egerer, M., and Satchell, K.J. (2015). *Vibrio cholerae* MARTX toxin heterologous translocation of beta-lactamase and roles of individual effector domains on cytoskeleton dynamics. Mol Microbiol. *95*, 590-604.

Egerer, M., and Satchell, K.J. (2010). Inositol hexakisphosphate-induced autoprocessing of large bacterial protein toxins. PLoS Pathog. *6*, e1000942.

Fehrenbacher, N., Bar-Sagi, D., and Philips, M. (2009). Ras/MAPK signaling from endomembranes. Mol Oncol. *3*, 297-307.

Fullner, K.J., Boucher, J.C., Hanes, M.A., Haines, G.K., 3rd, Meehan, B.M., Walchle, C., Sansonetti, P.J., and Mekalanos, J.J. (2002). The contribution of accessory toxins of *Vibrio cholerae* O1 El Tor to the proinflammatory response in a murine pulmonary cholera model. J Exp Med. *195*, 1455-1462.

Fullner, K.J., and Mekalanos, J.J. (1999). Genetic characterization of a new type IV-A pilus gene cluster found in both classical and El Tor biotypes of *Vibrio cholerae*. Infect Immun. *67*, 1393-1404.

Fullner, K.J., and Mekalanos, J.J. (2000). In vivo covalent cross-linking of cellular actin by the *Vibrio cholerae* RTX toxin. EMBO J. *19*, 5315-5323.

Gavin, H.E., Beubier, N.T., and Satchell, K.J. (2017). The Effector Domain Region of the *Vibrio vulnificus* MARTX Toxin Confers Biphasic Epithelial Barrier Disruption and Is Essential for Systemic Spread from the Intestine. PLoS Pathog. *13*, e1006119.

464 Gavin, H.E., and Satchell, K.J. (2015). MARTX toxins as effector delivery platforms. Pathog Dis.
465 *73*, ftv092.
466 Gavin, H.E., and Satchell, K.J.F. (2018). RRSP and RID Effector Domains Dominate Virulence
467 Impact of *Vibrio vulnificus* MARTX Toxin. J Infect Dis. jiy590.
468 Harrison, L.M., Rallabhandi, P., Michalski, J., Zhou, X., Steyert, S.R., Vogel, S.N., and Kaper,
469 J.B. (2008). *Vibrio cholerae* flagellins induce Toll-like receptor 5-mediated interleukin-8
470 production through mitogen-activated protein kinase and NF-kappaB activation. Infect Immun.
471 *76*, 5524-5534.
472 Heisler, D.B., Kudryashova, E., Grinevich, D.O., Suarez, C., Winkelman, J.D., Birukov, K.G.,
473 Kotha, S.R., Parinandi, N.L., Vavylonis, D., Kovar, D.R., et al. (2015). ACD toxin-produced actin
474 oligomers poison formin-controlled actin polymerization. Science. *349*, 535-539.
475 Kagnoff, M.F., and Eckmann, L. (1997). Epithelial cells as sensors for microbial infection. J Clin
476 Invest. *100*, 6-10.
477 Kim, B.S. (2018). The Modes of Action of MARTX Toxin Effector Domains. Toxins (Basel). *10*.
478 Kim, B.S., Gavin, H.E., and Satchell, K.J. (2015). Distinct roles of the repeat-containing regions
479 and effector domains of the *Vibrio vulnificus* multifunctional-autoprocessing repeats-in-toxin
480 (MARTX) toxin. MBio. *6*, e00324.
481 Kim, Y.R., Lee, S.E., Kook, H., Yeom, J.A., Na, H.S., Kim, S.Y., Chung, S.S., Choy, H.E., and
482 Rhee, J.H. (2008). *Vibrio vulnificus* RTX toxin kills host cells only after contact of the bacteria
483 with host cells. Cell Microbiol. *10*, 848-862.
484 Kudryashov, D.S., Cordero, C.L., Reisler, E., and Satchell, K.J. (2008). Characterization of the
485 enzymatic activity of the actin cross-linking domain from the *Vibrio cholerae* $MARTX_{Vc}$ toxin. J
486 Biol Chem. *283*, 445-452.
487 Kudryashova, E., Heisler, D.B., Williams, B., Harker, A.J., Shafer, K., Quinlan, M.E., Kovar,
488 D.R., Vavylonis, D., and Kudryashov, D.S. (2018). Actin Cross-Linking Toxin Is a Universal

Inhibitor of Tandem-Organized and Oligomeric G-Actin Binding Proteins. Curr Biol. *28*, 1536-1547 e1539.

Kwak, J.S., Jeong, H.G., and Satchell, K.J. (2011). *Vibrio vulnificus* rtxA1 gene recombination generates toxin variants with altered potency during intestinal infection. Proc Natl Acad Sci U S A. *108*, 1645-1650.

Lin, W., Fullner, K.J., Clayton, R., Sexton, J.A., Rogers, M.B., Calia, K.E., Calderwood, S.B., Fraser, C., and Mekalanos, J.J. (1999). Identification of a *Vibrio cholerae* RTX toxin gene cluster that is tightly linked to the cholera toxin prophage. Proc Natl Acad Sci U S A. *96*, 1071-1076.

Livak, K.J., and Schmittgen, T.D. (2001). Analysis of relative gene expression data using real-time quantitative PCR and the 2(-ΔΔC(T)) Method. Methods. *25*, 402-408.

Love, M.I., Huber, W., and Anders, S. (2014). Moderated estimation of fold change and dispersion for RNA-seq data with DESeq2. Genome Biol. *15*, 550.

Ma, A.T., and Mekalanos, J.J. (2010). In vivo actin cross-linking induced by *Vibrio cholerae* type VI secretion system is associated with intestinal inflammation. Proc Natl Acad Sci U S A. *107*, 4365-4370.

Mahida, Y.R., Makh, S., Hyde, S., Gray, T., and Borriello, S.P. (1996). Effect of *Clostridium difficile* toxin A on human intestinal epithelial cells: induction of interleukin 8 production and apoptosis after cell detachment. Gut. *38*, 337-347.

Martinez-Lopez, N., Athonvarangkul, D., Mishall, P., Sahu, S., and Singh, R. (2013). Autophagy proteins regulate ERK phosphorylation. Nat Commun. *4*, 2799.

Murciano, C., Lee, C.T., Fernandez-Bravo, A., Hsieh, T.H., Fouz, B., Hor, L.I., and Amaro, C. (2017). MARTX Toxin in the Zoonotic Serovar of *Vibrio vulnificus* Triggers an Early Cytokine Storm in Mice. Front Cell Infect Microbiol. *7*, 332.

Nogales-Cadenas, R., Carmona-Saez, P., Vazquez, M., Vicente, C., Yang, X., Tirado, F., Carazo, J.M., and Pascual-Montano, A. (2009). GeneCodis: interpreting gene lists through

514 enrichment analysis and integration of diverse biological information. Nucleic Acids Res. *37*,
515 W317-322.
516 Olivier, V., Haines, G.K., 3rd, Tan, Y., and Satchell, K.J. (2007). Hemolysin and the
517 multifunctional autoprocessing RTX toxin are virulence factors during intestinal infection of mice
518 with *Vibrio cholerae* El Tor O1 strains. Infect Immun. *75*, 5035-5042.
519 Olivier, V., Queen, J., and Satchell, K.J. (2009). Successful small intestine colonization of adult
520 mice by *Vibrio cholerae* requires ketamine anesthesia and accessory toxins. PLoS One. *4*,
521 e7352.
522 Peterson, L.W., and Artis, D. (2014). Intestinal epithelial cells: regulators of barrier function and
523 immune homeostasis. Nat Rev Immunol. *14*, 141-153.
524 Philippe, N., Alcaraz, J.P., Coursange, E., Geiselmann, J., and Schneider, D. (2004).
525 Improvement of pCVD442, a suicide plasmid for gene allele exchange in bacteria. Plasmid. *51*,
526 246-255.
527 Prochazkova, K., Shuvalova, L.A., Minasov, G., Voburka, Z., Anderson, W.F., and Satchell, K.J.
528 (2009). Structural and molecular mechanism for autoprocessing of MARTX toxin of Vibrio
529 cholerae at multiple sites. J Biol Chem. *284*, 26557-26568.
530 Qadri, F., Raqib, R., Ahmed, F., Rahman, T., Wenneras, C., Das, S.K., Alam, N.H., Mathan,
531 M.M., and Svennerholm, A.M. (2002). Increased levels of inflammatory mediators in children
532 and adults infected with *Vibrio cholerae* O1 and O139. Clin Diagn Lab Immunol. *9*, 221-229.
533 Queen, J., and Satchell, K.J. (2012). Neutrophils are essential for containment of *Vibrio*
534 *cholerae* to the intestine during the proinflammatory phase of infection. Infect Immun. *80*, 2905-
535 2913.
536 Rodriguez, B.L., Rojas, A., Campos, J., Ledon, T., Valle, E., Toledo, W., and Fando, R. (2001).
537 Differential interleukin-8 response of intestinal epithelial cell line to reactogenic and
538 nonreactogenic candidate vaccine strains of *Vibrio cholerae*. Infect Immun. *69*, 613-616.

539 Russell, R., Wang, H., Benitez, J.A., and Silva, A.J. (2018). Deletion of gene encoding the
540 nucleoid-associated protein H-NS unmasks hidden regulatory connections in El Tor biotype
541 *Vibrio cholerae*. Microbiology. *164*, 998-1003.
542 Satchell, K.J. (2015). Multifunctional-autoprocessing repeats-in-toxin (MARTX) Toxins of
543 *Vibrios*. Microbiol Spectr. *3*, VE-0002-2014.
544 Satchell, K.J., Jones, C.J., Wong, J., Queen, J., Agarwal, S., and Yildiz, F.H. (2016). Phenotypic
545 Analysis Reveals that the 2010 Haiti Cholera Epidemic Is Linked to a Hypervirulent Strain. Infect
546 Immun. *84*, 2473-2481.
547 Schwartz, M. (2004). Rho signalling at a glance. J Cell Sci. *117*, 5457-5458.
548 Sheahan, K.L., Cordero, C.L., and Satchell, K.J. (2004). Identification of a domain within the
549 multifunctional *Vibrio cholerae* RTX toxin that covalently cross-links actin. Proc Natl Acad Sci U
550 S A. *101*, 9798-9803.
551 Sheahan, K.L., and Satchell, K.J. (2007). Inactivation of small Rho GTPases by the
552 multifunctional RTX toxin from *Vibrio cholerae*. Cell Microbiol. *9*, 1324-1335.
553 Shen, A., Lupardus, P.J., Albrow, V.E., Guzzetta, A., Powers, J.C., Garcia, K.C., and Bogyo, M.
554 (2009). Mechanistic and structural insights into the proteolytic activation of *Vibrio cholerae*
555 MARTX toxin. Nat Chem Biol. *5*, 469-478.
556 Son, M.S., Megli, C.J., Kovacikova, G., Qadri, F., and Taylor, R.K. (2011). Characterization of
557 *Vibrio cholerae* O1 El Tor biotype variant clinical isolates from Bangladesh and Haiti, including a
558 molecular genetic analysis of virulence genes. J Clin Microbiol. *49*, 3739-3749.
559 Soriani, M., Bailey, L., and Hirst, T.R. (2002). Contribution of the ADP-ribosylating and receptor-
560 binding properties of cholera-like enterotoxins in modulating cytokine secretion by human
561 intestinal epithelial cells. Microbiology. *148*, 667-676.
562 Tabas-Madrid, D., Nogales-Cadenas, R., and Pascual-Montano, A. (2012). GeneCodis3: a non-
563 redundant and modular enrichment analysis tool for functional genomics. Nucleic Acids Res. *40*,
564 W478-483.

565 Weill, F.X., Domman, D., Njamkepo, E., Tarr, C., Rauzier, J., Fawal, N., Keddy, K.H., Salje, H.,
566 Moore, S., Mukhopadhyay, A.K., et al. (2017). Genomic history of the seventh pandemic of
567 cholera in Africa. Science. *358*, 785-789.
568 Woida, P.J., and Satchell, K.J.F. (2018). Coordinated delivery and function of bacterial MARTX
569 toxin effectors. Mol Microbiol. *107*, 133-141.
570 Woolery, A.R., Yu, X., LaBaer, J., and Orth, K. (2014). AMPylation of Rho GTPases subverts
571 multiple host signaling processes. J Biol Chem. *289*, 32977-32988.
572 Xu, H., Yang, J., Gao, W., Li, L., Li, P., Zhang, L., Gong, Y.N., Peng, X., Xi, J.J., Chen, S., et al.
573 (2014). Innate immune sensing of bacterial modifications of Rho GTPases by the Pyrin
574 inflammasome. Nature. *513*, 237-241.
575 Zhou, X., Gao, D.Q., Michalski, J., Benitez, J.A., and Kaper, J.B. (2004). Induction of interleukin-
576 8 in T84 cells by *Vibrio cholerae*. Infect Immun. *72*, 389-397.
577 Zhou, Y., Huang, C., Yin, L., Wan, M., Wang, X., Li, L., Liu, Y., Wang, Z., Fu, P., Zhang, N., et
578 al. (2017). N(epsilon)-Fatty acylation of Rho GTPases by a MARTX toxin effector. Science. *358*,
579 528-531.
580
581

582 **FIGURES AND FIGURE LEGENDS**

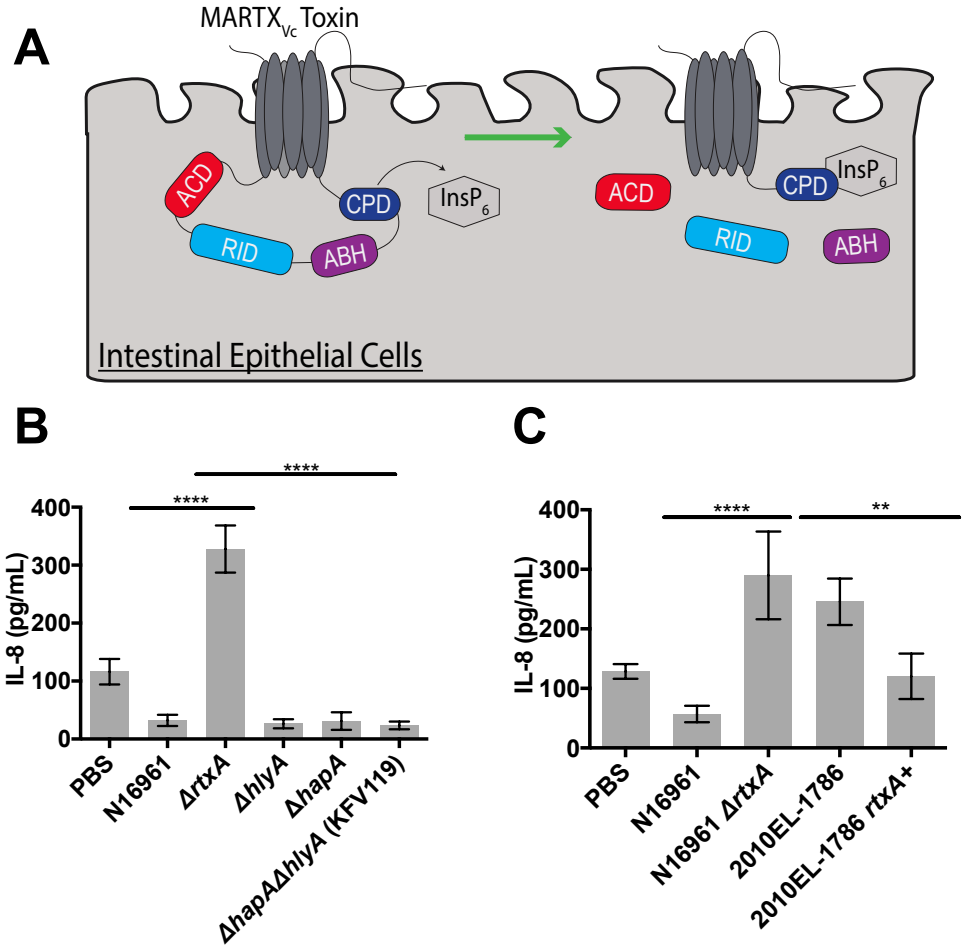

583

584 **Figure 1. The MARTX$_{Vc}$ toxin, and not other *V. cholerae* accessory toxins, suppress IL-8**

585 **in IECs**

586 (A) Schematic of MARTX$_{Vc}$ toxin activity in IECs. The MARTX$_{Vc}$ toxin utilizes N- and C-terminal

587 regions to form a pore in a target eukaryotic membrane and translocate the central effector

588 domains and CPD. CPD binds to InsP$_6$, which activates the domain autoproteolytic activity to

589 separate and release the three effector domains from the holotoxin.

590 (B, C) IL-8 secretion to the media from T84 intestinal cells inoculated with *V. cholerae* strains as

591 indicated Data are reported as means ± standard deviation (s.d.) (*n*=3-6) (** p<0.01,

592 ****p<0.0001, One-way ANOVA with multiple comparison's test).

593

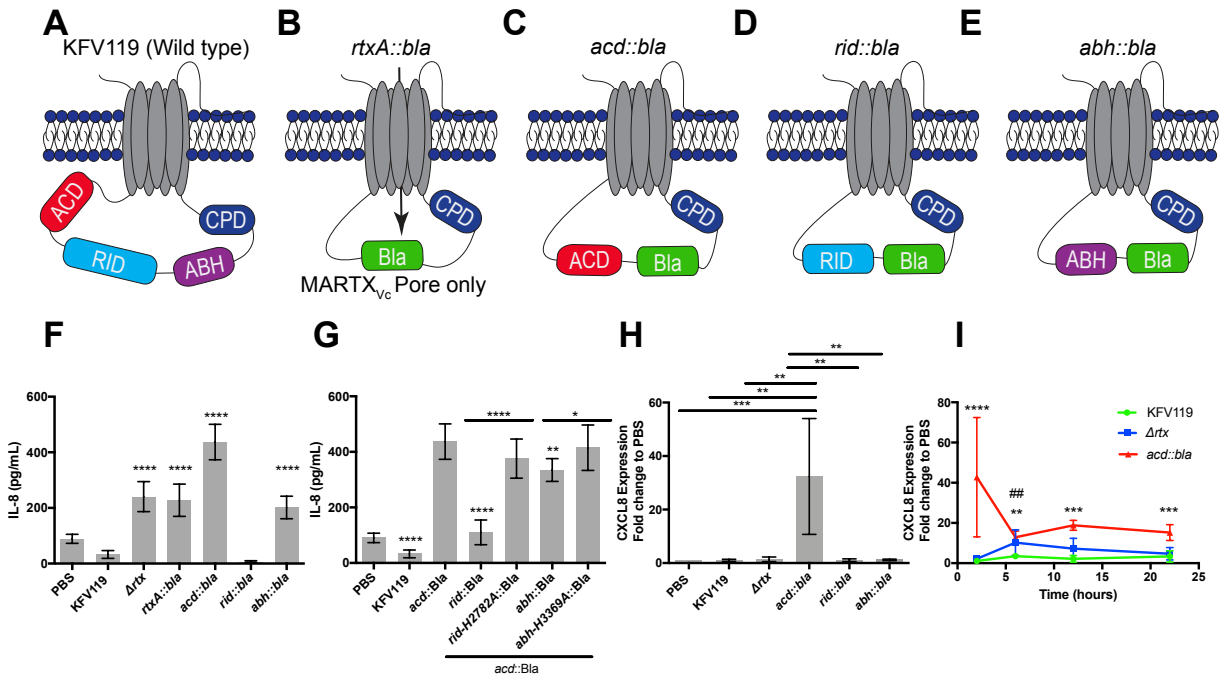

Figure 2. The MARTX$_{Vc}$ toxin effector domains, and not the pore, differentially regulate IL-8 secretion in IECs

(A-E) Schematics of MARTX$_{Vc}$ toxin effector arrangements in strains modified to translocate β-lactamase (Bla) and single effector gain-of-function strains (Dolores et al., 2015).

(F, G) IL-8 secretion measured from T84 intestinal cells inoculated with one or two *V. cholerae* effector-free Bla and single effector gain of function strains as indicated. Data are reported as means ± s.d. (*p<0.05, ** p<0.01, ****p<0.0001, One-way ANOVA with multiple comparisons).

(H, I) qPCR detection of *CXCL8* expression from T84 cells at (H) 120 min post-inoculation or (I) over 22 hours with *V. cholerae* strains as indicated. Data are reported as means ± s.d. (** p<0.01, ***p<0.001, ****p<0.0001, One-way ANOVA with multiple comparisons. For panel I, multiple comparisons between *acd::bla* and PBS were set as a normalized fold change of 1. ## p<0.001, One-way ANOVA with multiple comparisons between Δ*rtx* and PBS set as a normalized fold change of 1).

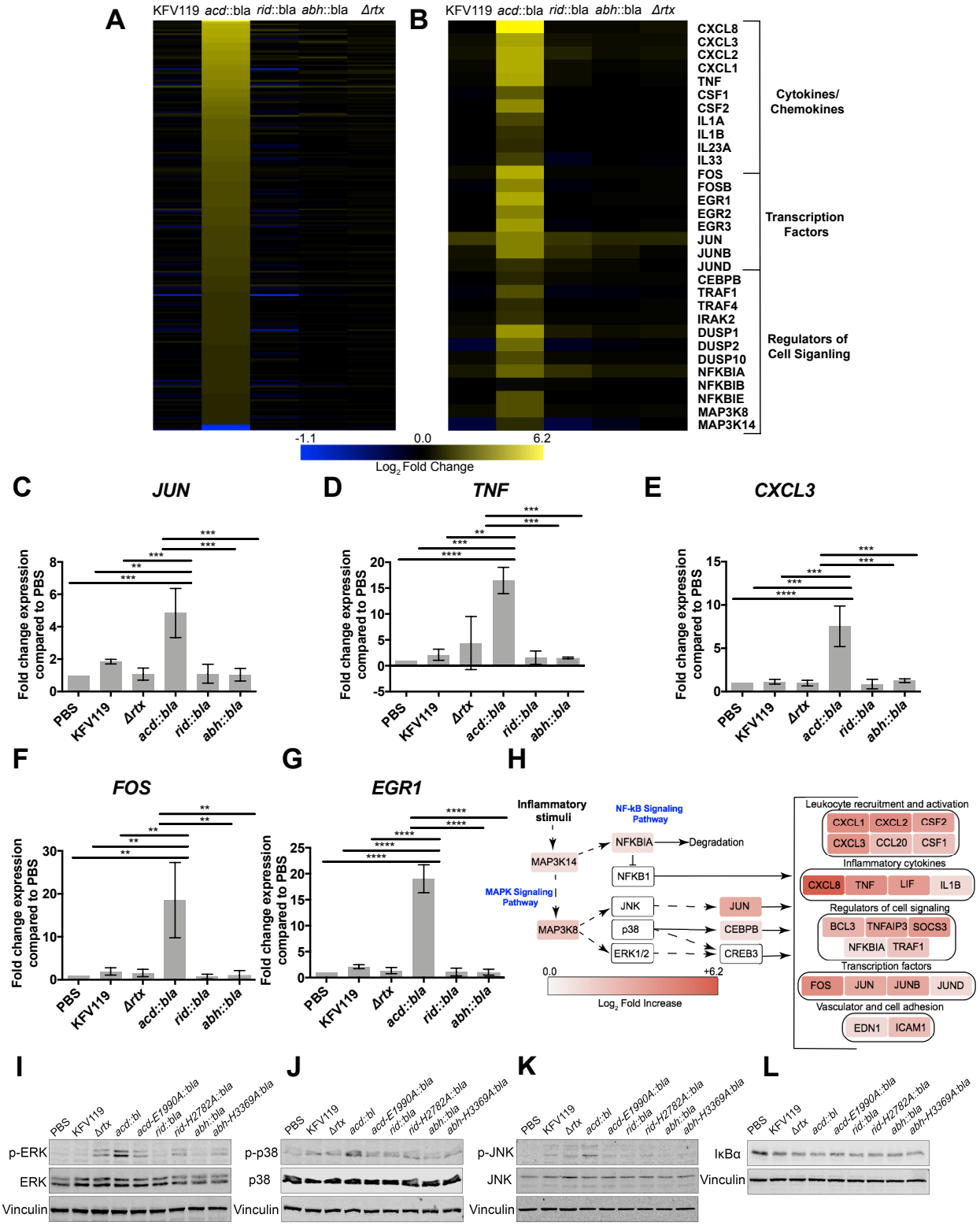

609

610 **Figure 3. ACD induces a global proinflammatory response that is silenced when**

611 **delivered with RID and ABH on the wild-type toxin**

(A, B) Heat maps of differentially expressed genes identified in RNA-sequencing analysis of T84 cells inoculated with *V. cholerae* strains as indicated. Heat maps represent statistically significant differentially expressed genes with a $-1 \leq 0 \leq 1$ $\log_2$ fold change cut off.

(C-G) qPCR validation of select differentially expressed genes. Data are reported as the mean ± s.d (** p<0.01, ***p<0.001, ****p<0.0001, One-way ANOVA with multiple comparisons between *acd::bla* and indicated strain. No other strains induced a statistically different response compared to the normalized PBS control or another strain).

(H) ACD significantly upregulated genes involved in regulation or downstream of the MAPK and NF-κB signaling pathways.

(I-L) Western blot analysis of (I) phospho-ERK, (J) phospho-p38, (K) phospho-JNK, and (L) IκBα degradation from T84 cells inoculated with *V. cholerae* strain as indicated. Blots are representative of three independent experiments.

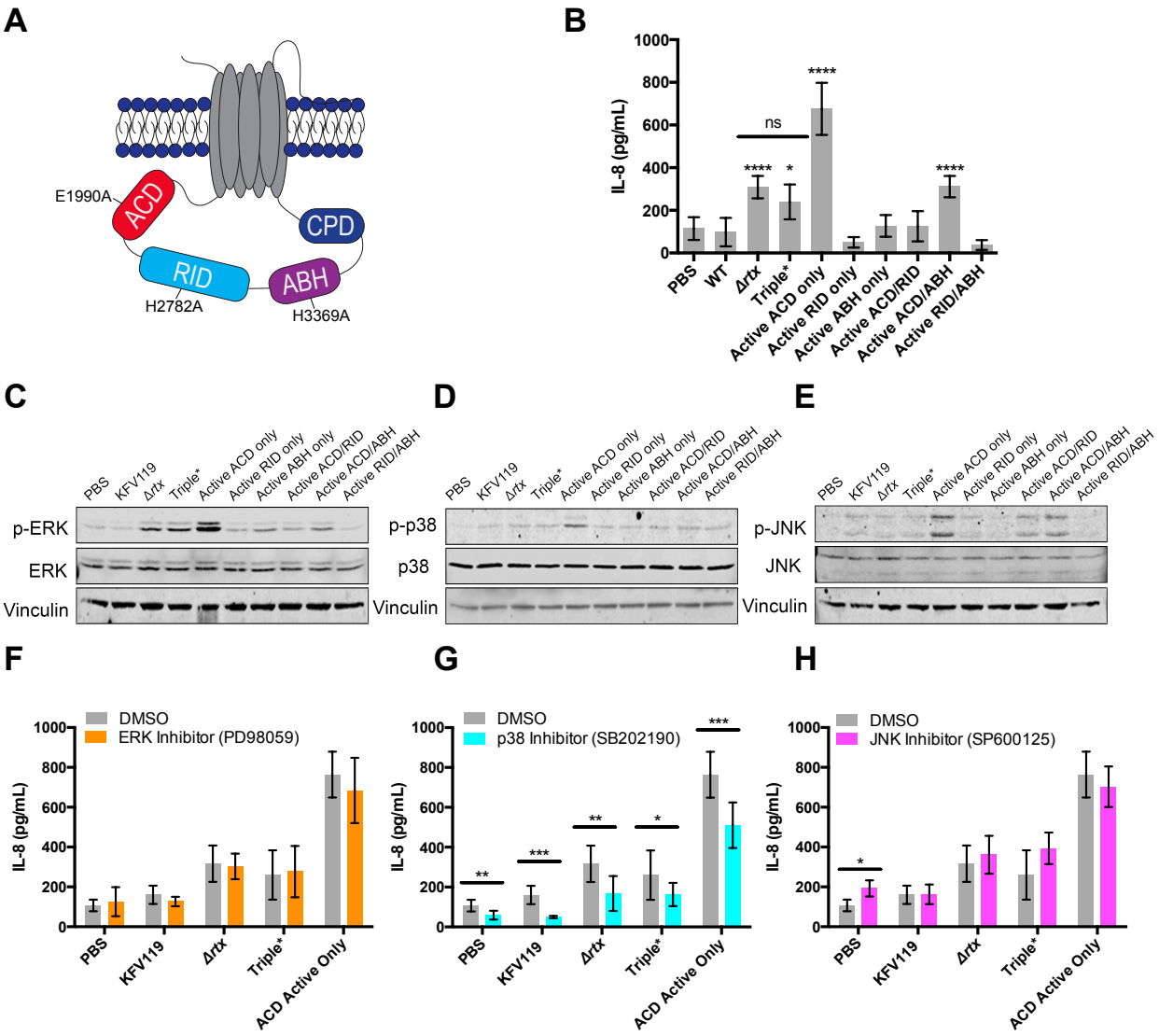

Figure 4. Both RID and ABH suppress ACD induced proinflammatory response

(A) Schematic of MARTX$_{Vc}$ toxin identifying catalytic residues mutated in single, double, and triple catalytically inactive MARTX$_{Vc}$ toxin effector strains.

(B) IL-8 secretion measured from T84 cells inoculated with *V. cholerae* strains as indicated. Data are reported as means ± s.d (*p<0.05, ** p<0.01, ****p<0.0001, One-way ANOVA with multiple comparisons).

632 (C-E) Western blot analysis of (C) phospho-ERK, (D) phospho-p38, and (E) phospho-JNK from
633 T84 cells inoculated with strains as indicated. Blots are representative of three independent
634 experiments.
635 (F-H) IL-8 secretion measured from T84 cells pre-treated with (F) ERK inhibitor PD98059, (G)
636 p38 inhibitor SB202190, and (F) JNK inhibitor SP600125. Data are reported as means ±
637 s.d.(*p<0.05, ** p<0.01, ****p<0.0001, Student's t-test).
638

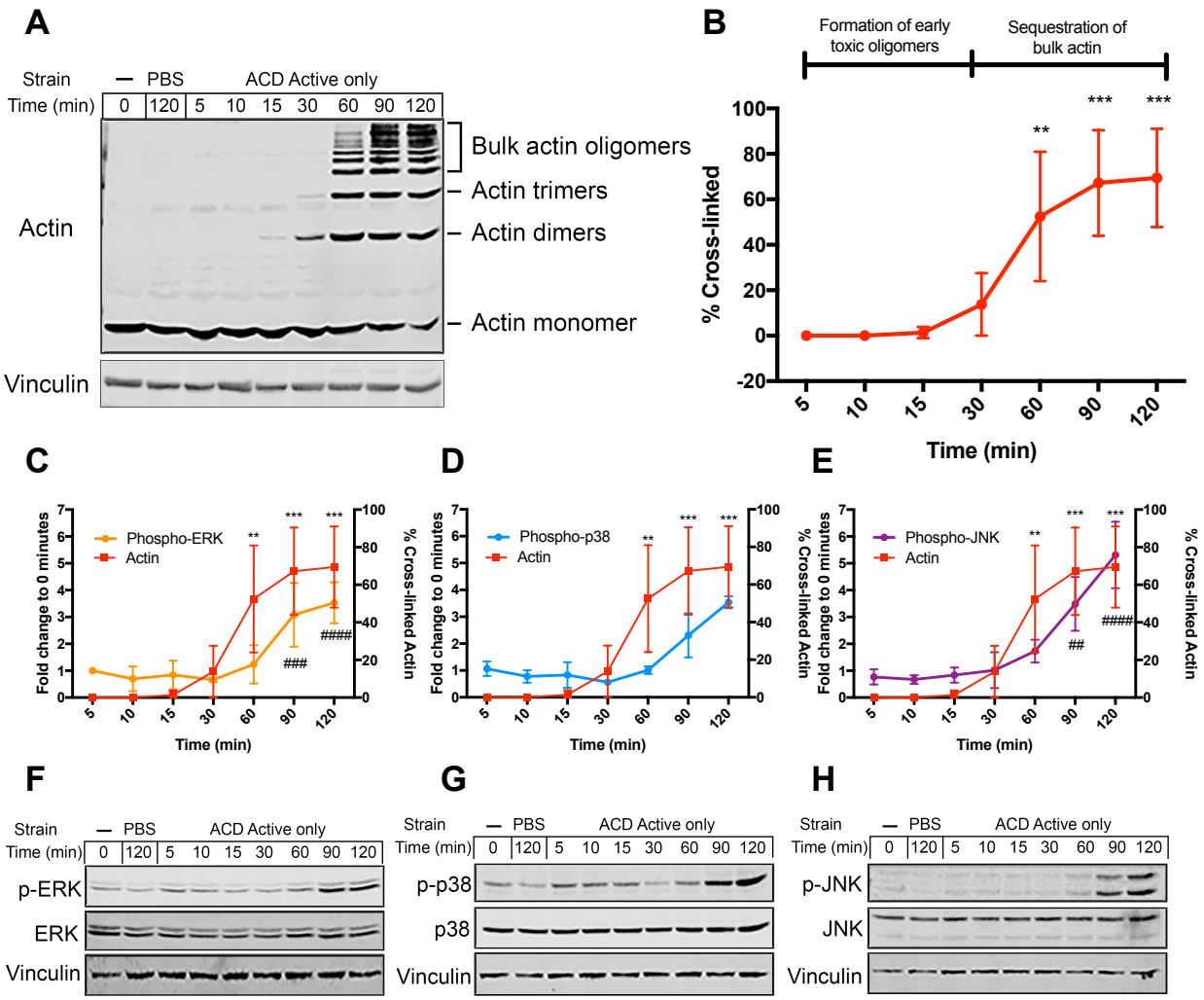

Figure 5. ACD activates proinflammatory MAPK signaling following sequestration of bulk actin

(A, B) Representative western blot and quantification (*n*=3) of actin cross-linking from T84 cells inoculated with the ACD only strain of *V. cholerae*. Actin oligomers start forming around 5 min to sequester actin binding proteins while significant cross-linking and sequestration of bulk actin and cytoskeleton destruction start forming at 60 min. Data are reported as means ± s.d.(** p<0.01, ***p<0.001, One-way ANOVA with multiple comparisons between indicated timepoints and 0% actin cross-linking from 0 min control).

(C - E) Fold change of (C) phospho-ERK (*n*=4), (D) phospho-p38 (*n*=2), and (E) phospho-JNK (*n*=3) compared to 0 min control quantified from western blot band densities from T84 cells

650 inoculated with the ACD Active only strain plotted with quantification of percent actin cross-
651 linked over the 120 min incubation. Data are reported as means ± s.d (** p<0.01, ***p<0.001,
652 One-way ANOVA with multiple comparisons between indicated timepoints and 0% actin cross-
653 linking from 0 min control from Figure 5B. ## p<0.01, ### p<0.001, #### p<0.0001, One-way
654 ANOVA with multiple comparisons between phospho-ERK/JNK at indicated timepoints and a 0
655 min control with a normalized fold change of 1). A third biological replicate was performed for
656 phospho-p38 quantification but the ACD Active only strain induced a stochastically high 273-fold
657 change compared to 0 min control (Figure S3A-B).
658 (F-H) Representative western blots (*n*=3-4) of (F) phospho-ERK, (G) phospho-p38, and (H)
659 phospho-JNK activation during 120 min bacterial challenge.
660

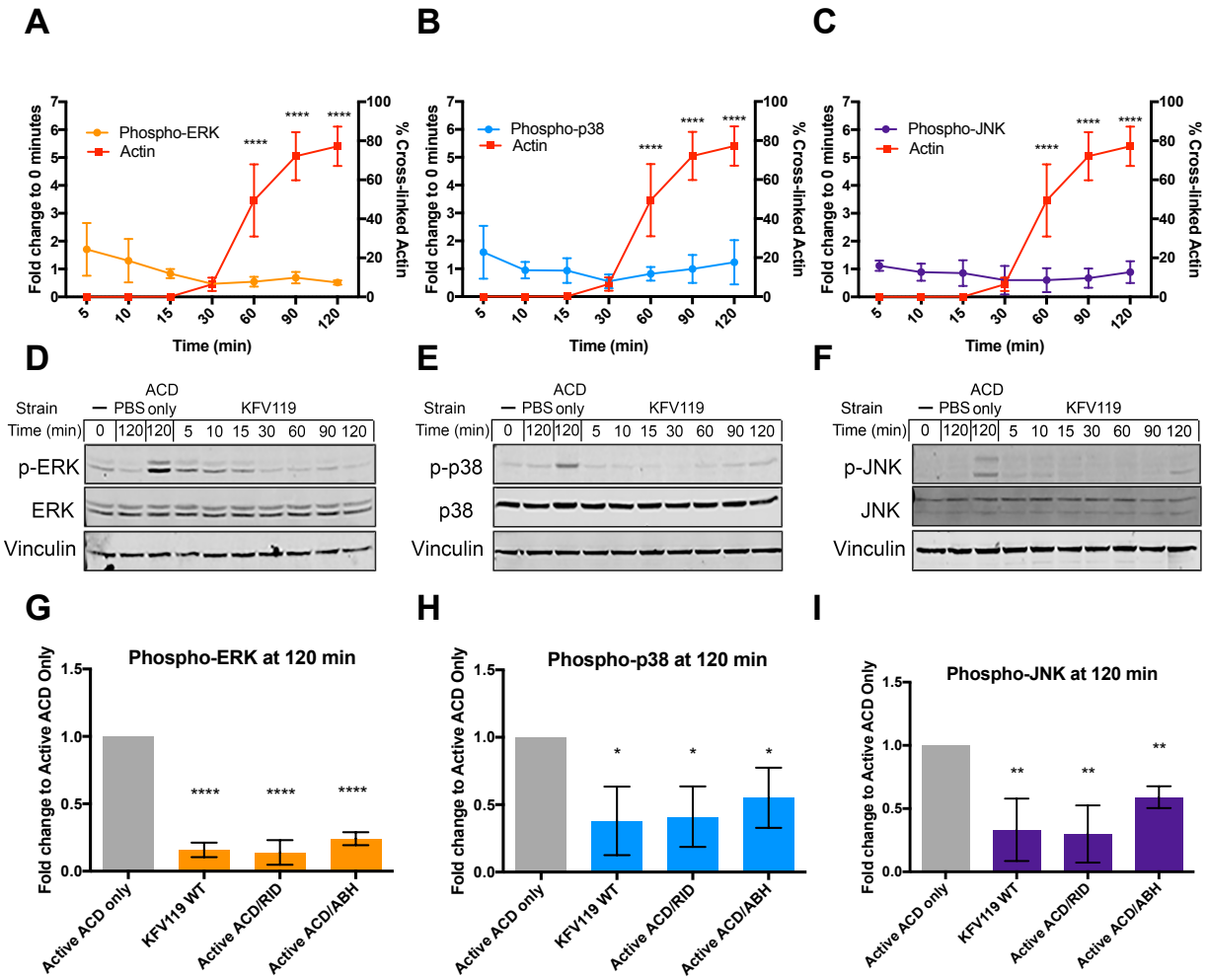

Figure 6. RID and ABH block MAPK signaling prior to host detection to ACD sequestration of bulk actin

(A–C) Fold change of (A) phospho-ERK, (B) phospho-p38, and (C) phospho-JNK compared to 0 min control quantified from western blot band densities from T84 cells inoculated with the WT KFV119 *V. cholerae* strain plotted with quantification of percent actin cross-linked over the 120 min incubation. Data are reported as the mean ± s.d.(****p<0.0001, One-way ANOVA with multiple comparisons between indicated timepoints and 0% actin cross-linking from 0 min control).

(D-F) Representative western blots of (D) phospho-ERK, (E) phospho-p38, and (F) phospho-JNK activation during 120 min bacterial challenge.

672 (G-I) Quantification of fold change in (G) phospho-ERK, (H) phospho-p38, and (I) phospho-JNK
673 compared to the Active ACD only strain at 120 minutes post-inoculation. Data are reported as
674 the mean ± s.d (*p<0.05, **p<0.01, ****p<0.0005, Student's t-tests compared to Active ACD only
675 strain). No statistically significant difference was observed between KFV119, ACD/RID Active,
676 or ACD/ABH Active strains compared to each other.
677

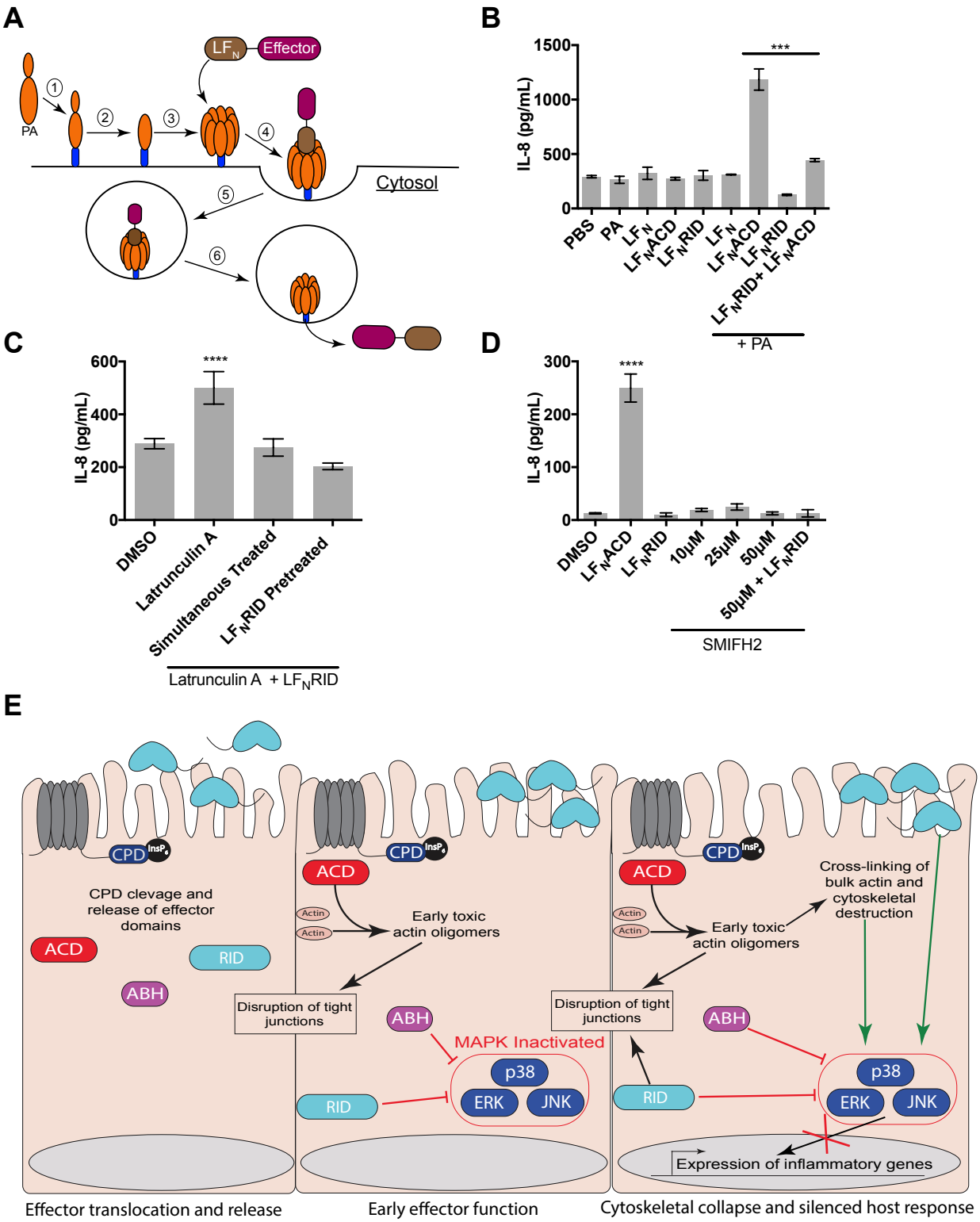

Figure 7. Cytoskeletal collapse, and not formation of toxic actin oligomers, activates proinflammatory response in IECs

(A) Schematic of LF_N- Effector intoxication. (1) PA binds to the anthrax toxin receptor. (2) PA is processed to its 63 kDa active form (PA_{63}). (3) PA_{63} oligomerizes to a heptamer complex. (4) The LF_N domain of the LF_N-MARTX effector fusion binds to the PA_{63} heptamer. (5) The LF_N-Effector + PA63 complex enters the cell through receptor mediated endocytosis. (6) Acidification of the vacuole promotes the PA_{63} heptamer to form a pore in the vacuole membrane to release LF_N-Effector fusion protein into the cytosol.

(B) IL-8 secretion measured from T84 intestinal cells treated with LF_N alone, LF_NACD, or LF_NRID in the presence or absence of PA. Data are reported as means ± s.d.(****p<0.0001, One-way ANOVA with multiple comparisons).

(C, D) IL-8 measured from T84 cells treated with (C) latrunculin A alone or (D) SMIFH2 in combination with LF_NRID in the presence of PA where indicated. Data are reported as means ± s.d.(*** p<0.001, ****p<0.0001, One-way ANOVA with multiple comparisons).

(E) Model of interplay between the $MARTX_{Vc}$ toxin multiple functions. (Left) $MARTX_{Vc}$ toxin effector domains are separated from the holotoxin. (Middle) During the early stages of effector activity, ACD actin cross-linking forms toxic actin oligomers to disrupt tight junctions. RID and ABH inactive MAPK signaling pathways. (Right). Inactivation of MAPK pathways blocks the inflammatory response to ACD destruction of the cytoskeleton and host detection of bacterial PAMPs.

699 **Materials and Methods**

700 Antibodies and chemical reagents

701 Antibodies used in this study include phospho-p44/p42 MAPK (ERK1/2) (Cell Signaling
702 Technology, #4337S), p44/p42 MAPK (ERK1/2) (Cell Signaling Technology, #4965S), phospho-
703 p38 MAPK (Cell Signaling Technology, #9211S), p38 MAPK (Cell Signaling Technology,
704 #9212S), phospho-SAPK/JNK (Cell Signaling Technology, #9255S), SAPK/JNK (Cell Signaling
705 Technology, #9252S), Vinculin (Cell Signaling Technology, #13901), IKBα (Cell Signaling
706 Technology, #9242S), Tubulin (Cell Signaling Technology, #2144), GAPDH (Santa Cruz, #sc-
707 25779), Actin (Sigma, #A2066), and LICOR IRDye 800CW/680LT secondary antibodies
708 (LICOR, #926-3221, #926-3211, #926-68070, #926-68071). Chemical reagents used in this
709 study were ERK MAPK inhibitor PD98059 (Cell Signaling Technology, #9900L), p38 MAPK
710 inhibitor SB202190 (Cell Signaling Technology, #S7067), JNK MAPK inhibitor SP600125
711 (Abcam, #120065), Latrunculin A (Millipore, #428021), and SMIFH2 (Fisher Scientific,
712 #440110).
713
714 Cell culture
715 T84 male colorectal carcinoma cells acquired from the American Type Culture Collection
716 (ATCC, #CCL-248) were cultured in Dulbecco's Modified Eagle Medium/Nutrient Mixture F-12
717 (DMEM/F12), GlutaMAX supplement (ThermoFisher Gibco, #10565018) with 10% (w/v) fetal
718 bovine serum (FBS, Gemini Bio-products, #900-108) and 0.1% penicillin/streptomycin
719 (ThermoFisher Gibco). Cells were maintained at 37°C in the presence of 5% CO_2.
720
721 Bacterial growth medium
722 Bacterial strains and plasmids used in this study are listed in Table S1. All *V. cholerae*
723 strains used in this study are derived from spontaneous streptomycin-resistant derivatives of

clinical isolates N16961 or 2010EL-1796. *V. cholerae* and *Escherichia coli* were grown on Luria-Bertani (LB) broth or agar. *V. cholerae* medium was supplemented with 100 μg mL^{-1} streptomycin, 2 μg mL^{-1} chloramphenicol, 100 μg mL^{-1} ampicillin, or 5% (w/v) sucrose as needed. *E. coli* growth medium was supplemented with 10 μg mL^{-1} chloramphenicol, 100 μg mL^{-1} ampicillin, or 50 μg mL^{-1} kanamycin as needed.

Treatment of cells with live bacteria

V. cholerae strains were grown at 30°C in LB medium supplemented with 100 μg mL^{-1} streptomycin. Overnight cultures were diluted 1:100 and grown at 30°C with shaking until exponential phase (OD_{600}≈0.40-0.60). Bacteria from 1 mL were pelleted by centrifugation and resuspended in phosphate buffered saline (PBS) to a final concentration of 5 x 10^8 bacterial cells mL^{-1}. T84 cells (seeded the day before into cell culture-treated plates) were twice washed with PBS and then media changed to antibiotic- and FBS-free DMEM/F12. Resuspended *V. cholerae* was added to media over cells (multiplicity of infection = 5). Inoculations were synchronized by centrifugation at 500 x*g* for 3 min. T84 cells were subsequently incubated at 37°C in the presence of 5% CO_2 until processed for downstream applications.

LF_NEffector intoxication of T84 cells

LF_N fusion proteins were expressed from pTCO24 (LF_NACD) and pKS119 (LF_NRID) and purified as previously described (Cordero et al., 2006; Sheahan and Satchell, 2007). In brief, *E. coli* containing BL21(DE3)(pMagic) with overexpression plasmids were grown in Terrific broth and expression of protein induced with 1 mM isopropyl β-D-thiogalactopyranoside at 25°C overnight. Bacteria were harvested in Buffer A (10mM Tris, 500 mM NaCl pH 8.3), lysed by sonication, and lysate clarified by centrifugation at 16,0000 x*g* for 30 min. The 6xHis-tagged recombinant proteins were purified using Ni-NTA HisTrap column followed by size-exclusion

749 chromatography using a Superdex 75 column in Buffer A with 5 mM β-mercaptoethanol using
750 the ÄKTA protein purification system (GE Healthcare). Proteins were stored in 10% glycerol at
751 -80°C.

752 For intoxication of cells, media was replaced over 10^5 cells previously seeded in a 12-well
753 plate. 31.7 nM PA alone (List Labs, #171E) or in the presence of 13.6nM LF_N, LF_N-ACD, or LF_N-
754 RID was added to media and cells were incubated for 20 hr at 37°C in the presence of 5% CO_2.
755 For co-intoxication of 13.6 nM LF_NACD and LF_N-RID, 3x excess PA was used to ensure equal
756 translocation of both effectors.

757

758 Construction of pDS132 *sacB*-counterselectable plasmids

759 Fragments (gBlocks) containing either the ACD E1990A mutation or the ABH H3369A
760 mutation along with 500 base pairs up and downstream from the mutations were commercially
761 synthesized. Each fragment also has additional secondary silent mutations to introduce novel
762 MfeI and PstI restriction sites near the E1990A and H3369A mutations, respectively. Sequences
763 are listed in Table S2. Fragments were cloned into pDS132 digested with SphI (New England
764 Biolabs, #R3182S) using Gibson Assembly (New England Biolabs, #E2611S) according to
765 manufacturer's instructions. Plasmids were recovered and propagated in DH5αλ*pir* on LB
766 supplemented with chloramphenicol and confirmed by sequencing.

767

768 Transfer of E1990A, H2782A, and H3369A mutations to the *V. cholerae* chromosome

769 The ACD E1990A and ABH H3369A mutations on the above pDS132-based plasmids
770 were transferred to SM10λ*pir*. These mutations or the RID H2782A mutation from pSA129 were
771 transferred to the *V. cholerae* chromosome by conjugation followed by *sacB*-dependent
772 counterselection for double homologous recombination as previously described (Ahrens et al.,
773 2013; Dolores et al., 2015). To confirm recombinants gained the desired mutations, regions

774 corresponding to the mutations were amplified by PCR, digested with the introduced novel
775 restriction site, and products were separated on agarose gel. Presence of introduced mutations
776 were also confirmed by sequencing.
777
778 IL-8 enzyme-linked immunosorbent assay (ELISA)
779 1- to 2 x 10^5 T84 cells seeded in a 12-well tissue culture treated plate were treated as
780 described above for 2 hr. Media from inoculated cells was removed, cells were washed once
781 with warm PBS and media changed to DMEM12 GlutaMAX media supplemented with serum,
782 pen-strep, and 100 μg mL^{-1} gentamicin. Cells were incubated for an additional 20 hr at 37°C in
783 the presence of 5% CO_2. For IL-8 chemical inhibitor studies, 10 μM of MAPK inhibitor or 0.33%
784 DMSO control were added to T84 cells one hour prior to bacterial challenge. Inhibitors were
785 reapplied following 2 hr bacterial challenge. Media from the T84 cells was harvested and spun
786 down at 20,000x*g* for 1 min at 4°C and supernatant was collected. Concentration of IL-8 in cell
787 media was measured using the IL-8 Human Matched Antibody Pair ELISA kit (ThermoFisher,
788 #CHC1303) following manufacturer's instructions.
789
790 Western blot analysis of actin crosslinking and cell signaling pathways
791 1 x 10^6 T84 cells in a 6-well tissue culture dish were treated with various *V. cholerae*
792 strains as described above for 2 hr. Cells were washed once with cold PBS and removed from
793 the plate in 150 μL lysis buffer (150 mM NaCl, 20 mM TRIS pH 7.5, 1% Triton X-100, and Pierce
794 Protease and Phosphatase inhibitor added prior to use) using a cell scrapper. Lysates were
795 incubated on ice for 15 min and then clarified by centrifugation at 20,000*xg* at 4°C for 10 min.
796 Concentration of protein in the collected supernatant fluid determined using the bicinchoninic
797 (BCA) assay (ThermoFisher, #23227). Normalized samples were boiled for 5 min at 95°C in
798 SDS loading buffer and protein separated on either a 10% or 15% SDS-polyacrylamide gel.

Proteins were transferred to nitrocellulose membranes and blocked in TBS (10 mM Tris pH=7.4, 150 mM NaCl) with 5% (w/v) milk for 1 hour. Membranes were washed with TBS and then incubated in indicated primary antibodies 1:1000 in TBS with 5% (w/v) bovine serum album (BSA, Fisher Bioreagents) overnight at 4°C. Membranes were washed with TBS and probed in 1:10,000 IRDye 800CW/680LT secondary antibody for 1 hour before being washed again and imaged using the LI-COR Bioscience Odyssey imaging system. Quantification of band density was conducted using Fiji/ImageJ.

RNA-seq

The stranded mRNA-seq was conducted in the Northwestern University NUSeq Core Facility. Briefly, total RNA examples were checked for quality using RINs generated from Agilent Bioanalyzer 2100. RNA quantity was determined with Qubit fluorometer. The Illumina TruSeq Stranded mRNA Library Preparation Kit was used to prepare sequencing libraries from 750 ng of high-quality RNA samples (RIN=10). The Kit procedure was performed without modifications. This procedure includes mRNA purification and fragmentation, cDNA synthesis, 3' end adenylation, Illumina adapter ligation, library PCR amplification and validation. Illumina NextSeq 500 Sequencer was used to sequence the libraries with the production of single-end, 75 bp reads.

The quality of DNA reads, in fastq format, was evaluated using FastQC. Adapters were trimmed, and reads of poor quality or aligning to rRNA sequences were filtered. The cleaned reads were aligned to the human reference genome using STAR (Dobin et al., 2013). Read counts for each gene were calculated using htseq-count (Anders et al., 2015). Normalization and differential expression were determined using DESeq2 (Love et al., 2014). The cutoff for determining significantly differentially expressed genes was an FDR-adjusted p-value less than 0.05. A pathway analysis was performed on both gene lists using GeneCoDis (Carmona-Saez

824 et al., 2007; Nogales-Cadenas et al., 2009; Tabas-Madrid et al., 2012) to identify pathways that
825 are enriched with genes that are upregulated and downregulated.
826
827 Quantitative RT-PCR
828 1 x 10^6 T84 cells in a 6-well tissue culture treated plate were treated with *V. cholerae* as
829 described above. At indicated time points, mRNA was harvested using the Qiagen RNeasy kit
830 (Qiagen, #74014) following manufacturer's instructions. RNA isolated was measured using a
831 Nano-drop 100 spectrophotometer. Reverse transcription was performed using random
832 hexamers (Roche) and Superscript III Reverse Transcriptase (Invitrogen, #18080044) in the
833 presence of RNase OUT (Invitrogen, #10777019) or RNasin (Promega, #N2611) under the
834 following conditions: 25°C for 5 min, then 55°C for 60 min, 95°C for 5 min. Remaining RNA was
835 hydrolyzed using 1 N NaOH. Quantitative PCR was performed using iQ SYBR Green supermix
836 (Bio-Rad, #1708880) on the iQ5 Multicolor RealTime PCR Detection System using gene
837 specific primers indicated in Table S3. Relative change in gene expression compared to PBS
838 control was determined the ΔΔCT method (Livak and Schmittgen, 2001).
839
840 Quantification and statistical analysis
841 All experiments were done at least in triplicate and quantitative results are reported as the
842 mean ± standard deviation (s.d.). Statistical analysis was performed using GraphPad Prism v6.0
843 as detailed in the figure legends. Statistical differences in ELISA and qPCR results were
844 determined by one-way ANOVA followed by multiple comparison's test. Statistical difference in
845 results comparing suppression of ERK, p38, and JNK signaling by various *V. cholerae* strains
846 compared to the ACD Active only strain were determined using Student's t-tests.
847
848

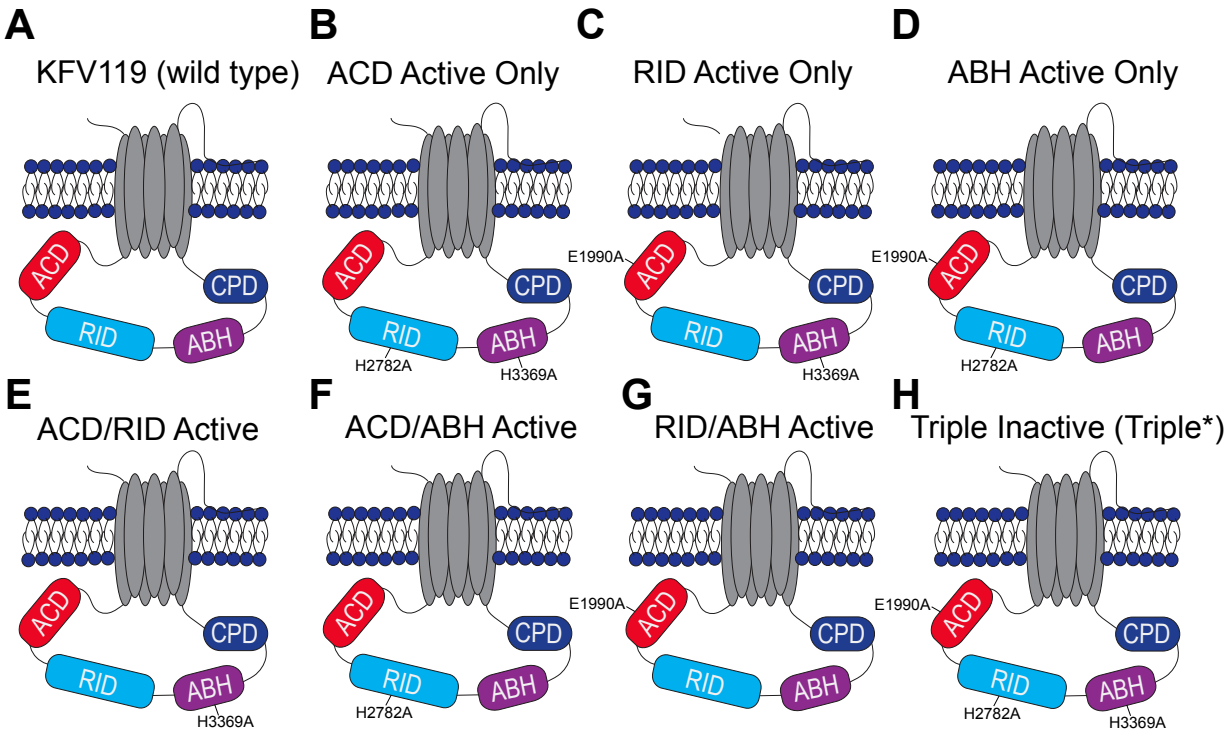

Figure S1. Schematic of single and double catalytically active MARTX$_{Vc}$ toxin effector strains and triple inactive MARTX$_{Vc}$ toxin effector strain.

(A) Wild type toxin. (B) RID Active only strain with RID and ABH catalytically inactive. (C) RID Active only strain with ACD and ABH catalytically inactive. (D) ABH Active only strain with ACD and RID catalytically inactive. (E) ACD/RID active strain with only ABH catalytically inactive. (F) ACD/ABH Active strain with only RID catalytically inactive. (G) RID/ABH Active strain with only ACD catalytically inactive. (H) Triple inactive strain (Triple*) with all three effectors catalytically inactive.

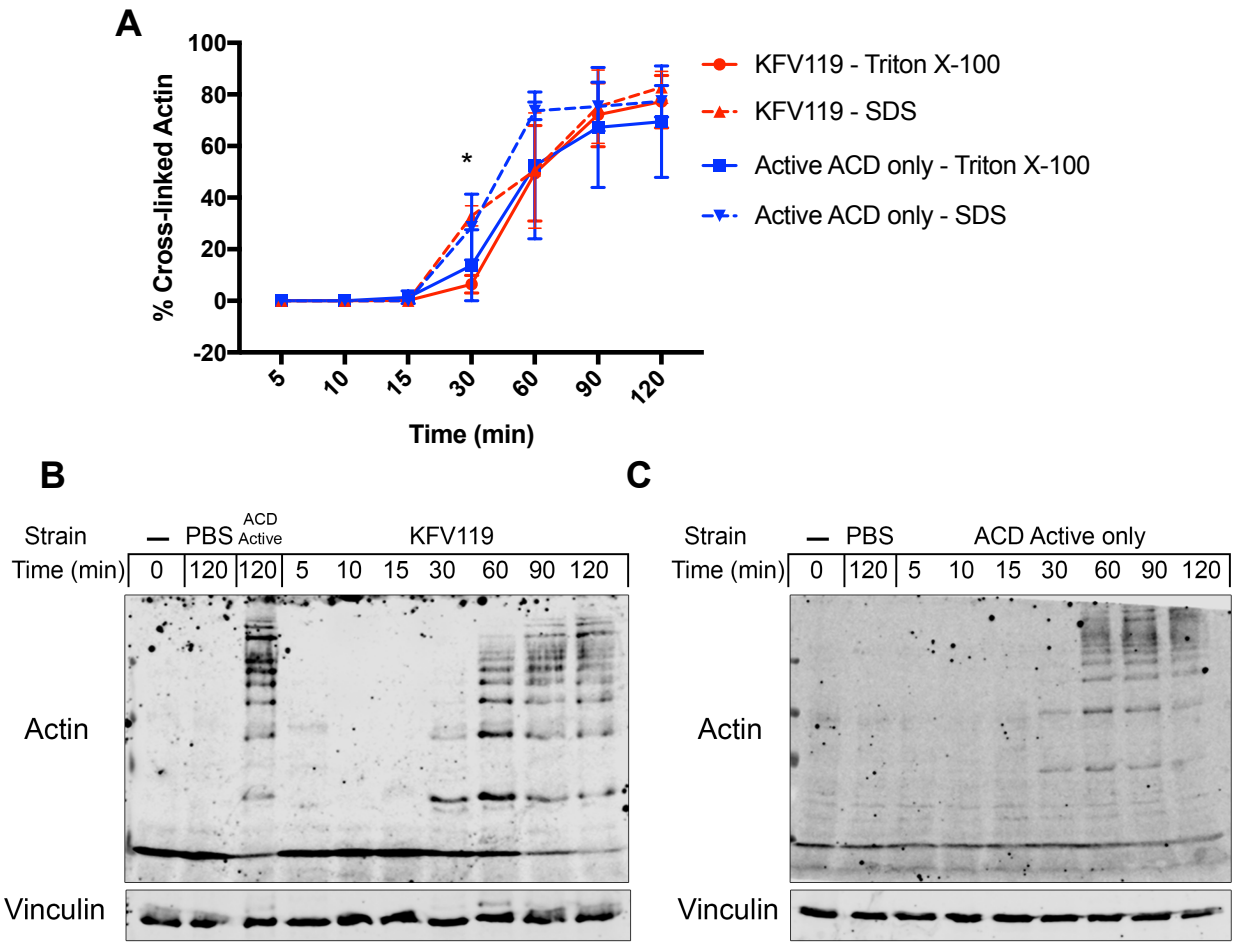

Figure S2. Cells harvested in Triton X-100 lysis buffer for assessment of MAPK phosphorylation underestimates the rate of actin cross-linking further supporting that extensive cross-linking occurs ahead of inflammation.

(A) Quantification of actin cross-linking from T84 cells treated with KFV119 or the ACD Active Only strain with washed cells being lysed and collected in Triton X-100 lysis buffer followed by centrifugation and protein quantification or by direct resuspension and boiling in 2x SDS loading buffer. Data reported as mean ± s.d.

(B) Representative western blot of actin cross-linking from T84 cells inoculated with KFV119 and samples collected in SDS loading buffer.

871 (C) Representative western blot of actin cross-linking form T84 cells inoculated with the
872 ACD Active only strain and samples collected in SDS loading buffer.
873 Triton X-100 lysis underestimates actin cross-linking at early time points further
874 supporting that extensive cross-linking activate the inflammatory response. Specifically,
875 there is a statistically significant increase in actin cross-linking observed when KFV119
876 treated cells were lysed using SDS loading buffer compared to Triton X-100 at 30
877 minutes (*$p<0.05$, Two-way ANOVA with multiple comparisons). However, no significant
878 difference was observed at any time point between the two methods when cells were
879 treated with the ACD Active only strain. No significant difference was observed
880 comparing samples treated with either KFV119 and the ACD Active only strain when
881 using either method.
882
883

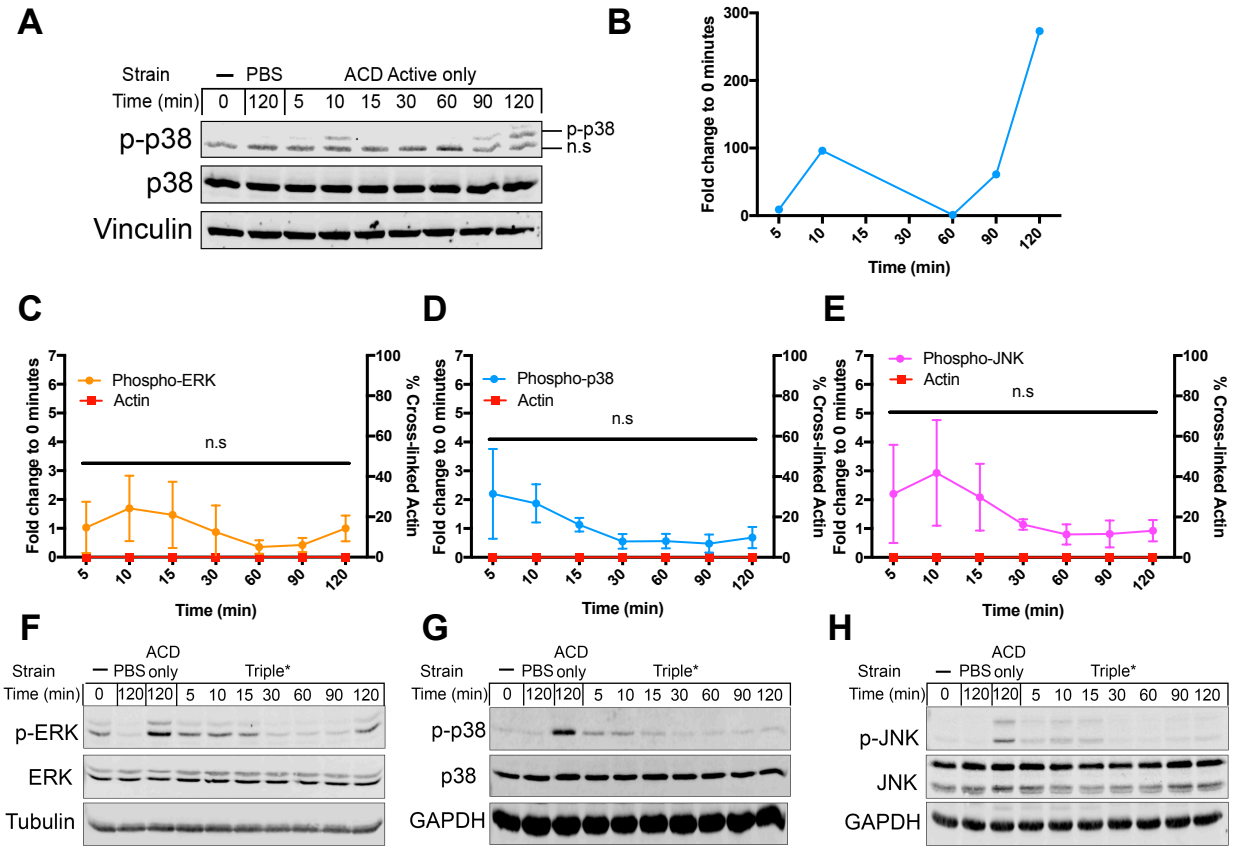

Figure S3. MAPK activation over 120 min challenge with the triple inactive (Triple*) MARTX$_{Vc}$ toxin effector strain.

(A) Western blot analysis of p-38 activation by the ACD only strain 273-fold times higher at 120 min compared to the 0 min control. Non-specific bands are indicated as n.s.

(B) Quantification of p-38 activation from western blot presented in panel A.

(C-E) Fold change of (C) phospho-ERK, (D) phospho-p38, and (E) phospho-JNK compared to 0 min control quantified from western blot band densities from T84 cells inoculated with the Triple* *V. cholerae* strain plotted with quantification of percent actin cross-linked over the two hour incubation.

(F-H) Representative western blots of (G) phospho-ERK, (H) phospho-p38, and (I) phospho-JNK activation during 120 min bacterial challenge.

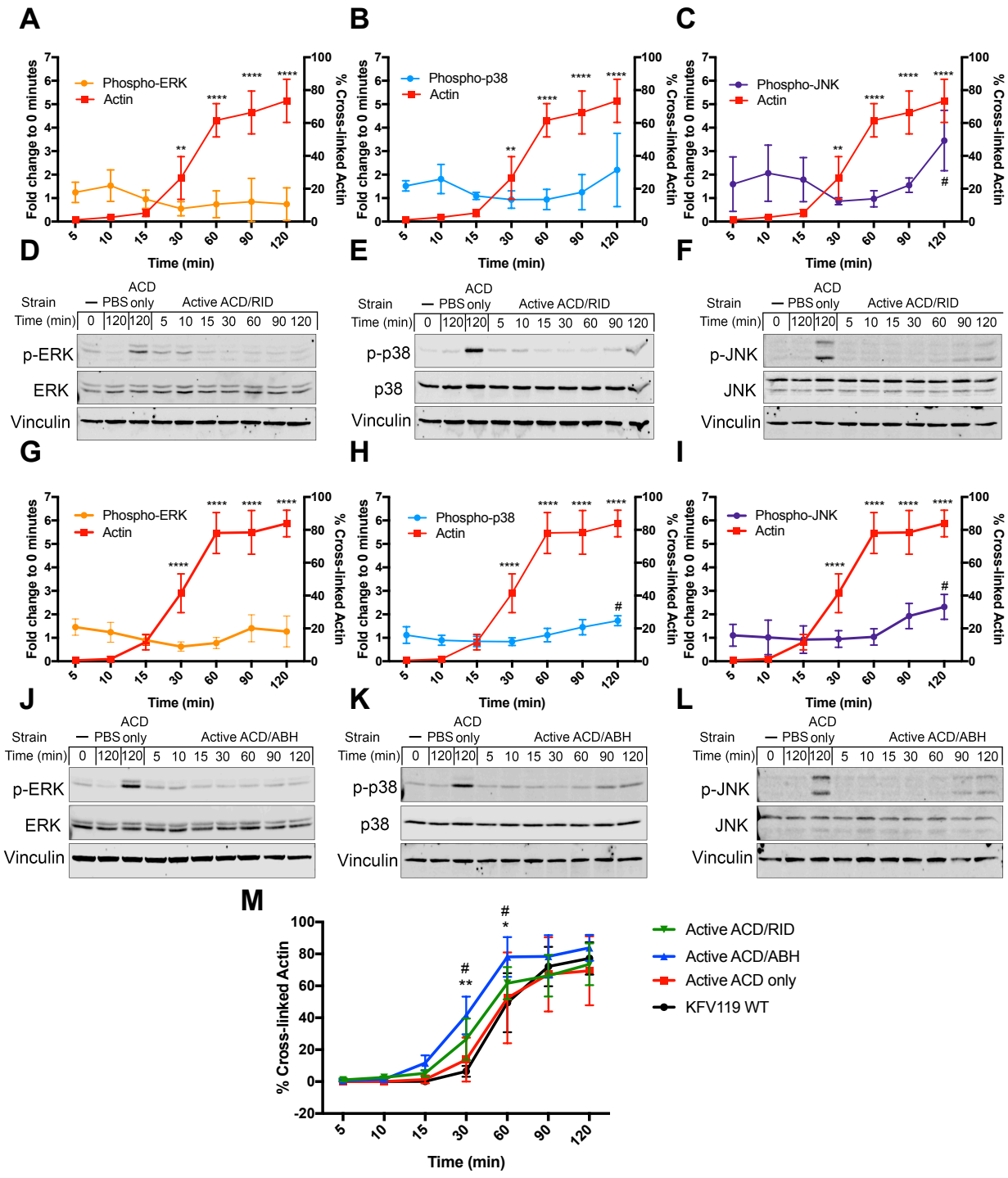

Figure S4. RID and ABH block MAPK signaling prior to host detection of sequestration of bulk actin without modulating ACD activity.

(A-C) Fold change of (A) phospho-ERK, (B) phospho-p38, and (C) phospho-JNK compared to 0 min control quantified from western blot band densities from T84 cells inoculated with the ACD/RID active *V. cholerae* strain plotted with quantification of percent actin cross-linked over the two hour incubation (**p<0.01, ****p<0.0001, One-way ANOVA with multiple comparisons between indicated timepoints and 0% actin cross-linking from 0 min control. # p<0.05, One-way ANOVA with multiple comparisons between phospho-JNK at indicated timepoint and a 0 min control with a normalized fold change of 1).

(D-F) Representative western blots of (D) phospho-ERK, (E) phospho-p38, and (F) phospho-JNK activation during 120 min bacterial challenge.

(G-I) Fold change of (G) phospho-ERK, (H) phospho-p38, and (I) phospho-JNK compared to 0 min control quantified from western blot band densities from T84 cells inoculated with the ACD/ABH active *V. cholerae* strain plotted with quantification of percent actin cross-linked over the 120 min incubation. (****p<0.0001, One-way ANOVA with multiple comparisons between indicated timepoints and 0% actin cross-linking from 0 min control. # p<0.05, One-way ANOVA with multiple comparisons between phospho-p38/JNK at indicated timepoints and a 0 min control with a normalized fold change of 1).

(J-L) Representative western blots of (J) phospho-ERK, (K) phospho-p38, and (L) phospho-JNK activation during 120 min bacterial challenge.

(M) Comparison of percent actin cross-linking during 120 min bacterial challenge of ACD positive *V. cholerae* strains (* p<0.05, ** p<0.01 Two-way ANOVA with multiple comparisons between KFV119 and Active ACD/ABH, #p<0.05, Two-way ANOVA with multiple comparisons between Active ACD only and Active ACD/ABH).

923

Table S1. Bacterial strains and plasmid used in study.

Designation	Relevant Description	Source
E. coli		
BL21(DE3)(pMagic)	Protein overexpression, Km^R	A. Joachimiak (Argonne National Laboratory)
DH5αλ*pir*	Plasmid cloning	Lab stock
SM10λ*pir*	Conjugation to *V. cholerae,* Sm^R	Lab stock
V. cholerae		
N16961Sm	El Tor O1, Wild-type, Sm^R	(Lin et al., 1999)
KFV43	N16961*ΔhapA*	(Fullner and Mekalanos, 1999)
VOV21	N16961*ΔhlyA*	(Olivier et al., 2007)
CW123	N16961*ΔrtxA*	(Sheahan et al., 2004)
KFV119	N16961*ΔhlyAΔhapA*	(Dolores et al., 2015)
JD23	KFV119*ΔrtxABCD*	(Dolores et al., 2015)
JD1	KFV119 *rtxA::bla*	(Dolores et al., 2015)
JD20	KFV119 *acd::bla*	(Dolores et al., 2015)
JD19	KFV119 *rid::Bla*	(Dolores et al., 2015)
JD21	KFV119 *rid-H2782A::bla*	(Dolores et al., 2015)
JD2	KFV119 *abh::bla*	(Dolores et al., 2015)
JD15	KFV119 *abh-H3369A::bla*	(Dolores et al., 2015)
2010EL-1786	Atypical El Tor O1, Wild-type, Sm^R	ATCC #BAA-2163
JD16	2010EL-1786ΩpJD22 (2010EL-1786 *rtxA*+)	(Dolores and Satchell, 2013)
PJWV1	KFV119 *rtxA-E1990A* (RID/ABH Active)	This Study
PJWV2	KFV119 *rtxA-H2782A* (ACD/ABH Active)	This Study
PJWV3	KFV119 *rtxA-H3369A* (ACD/RID Active)	This Study
PJWV4	KFV119 *rtxA-E1990A-H2782A* (ABH Active Only)	This Study
PJWV5	KFV119 *rtxA-E1990A-H3369A* (RID Active Only)	This Study
PJWV6	KFV119 *rtxA-H2782A-H3369A (ACD Active Only)*	This Study
PJWV7	KFV119 *rtxA-E1990A-H2782A-H3369A* (Triple*)	This Study
Plasmids		
pTCO24	Overexpression of LF_N-ACD, Amp^R	(Cordero et al., 2006)

pKS119	Overexpression of LF_N-RID, Amp^R	(Sheahan and Satchell, 2007)
pSA129	*sacB* counterselection cloning vector pWM91with *rtxA* with fragment of H2782A codon change, Amp^R	(Ahrens et al., 2013)
pDS132	*sacB* counterselection cloning vector, oriR6K, oriT, Chl^R	(Philippe et al., 2004)
pPJW4	pDS132 with fragment of *rtxA* with E1990A codon change, Chl^R	This Study
pPJW5	pDS132 with fragment of *rtxA* with H3369A codon change, Chl^R	This Study

924
925

926
927 **Table S2. Sequences of gBlocks used to clone into pDS132 and modify ACD (E1990A)**

928 **and ABH (H3369A) effector domains of *rtxA* on the *V. cholerae* genome.**

Mutation	Sequence (5'-3') (introduce codon changes highlighted)
ACD E1990A	CCCAAGCTTCTTCTAGAGGTACCGCATGCCAAGCACAAGCCGATGCTC AAGGTGCTAAACAAAACGAAGGTGATCGTCCTGATCGTCAAGGCGTGA CTGGTAGTGGCCTTTCGGGTAATGCTCATAGTGTGGAAGGCGCTGGCG AAACAGACAGTCATGTCAACACCGACAGCCAAACCAACGCCGATGGCC GATTCAGTGAAGGTTTAACCGAACAAGAGCAAGAAGCGCTAGAAGGTG CGACCAACGCAGTGAACCGTTTGCAAATTAACGCAGGTATTCGAGCGA AAAACAGCGTTAGCAGTATGACTTCTATGTTCTCTGAAACAAATAGCAAG AGCATTGTTGTTCCTACCAAAGTCTCGCCTGAACCAGAGCGCCAAGAAG TGACTCGTAGAGACGTCCGTATCTCAGGGGTGAACCTCGAAAGTCTAA GTGCGGTACAGGGAAGTCAACCAACGGGTCAACTGGCTTCGAAAAGTG TCCCCGGATTTAAAAGCCATTTCGCATCGACATCAATTGGTATA**GCA**AA TGAGTTATCCGGTCTGGTGGTGGTTTTACCGAAAAACTCAGCGCAGACT TTTGGCTATGTGCATGATTCACAAGGTAACCCATTGTTCATGCTAACCAA GGATATGAATCAAGGTGGTTATAGCAACCCAGTGGGTATCAATGATATT CAAGGGGTGAACAACTGGCAGACGCATACGATTGAACTGGTTACATATC CTAGTGAAATCAGTGATACAGCAGCGGTTGAAAGTCGTAAAGAGGCAAT GCTATGGCTTGCGAAAGAGTTTACCGATCATATCAATCAGTCTAACCAC CAAAGCTTACCTCATTTAGTGAGTGATGACGGTCGTTTCACTCTGGTTAT ATCGAACTCTAAGCATCTTATTGCGGCGGGTAACGGAACCTCTATTGAT GCACAAGGCAAGACCATAGGAATGACCCCTAGTGGCCAACAAGCAACA ATGGCGATCAGTGCGAAAGAATTTGGTACAAGCTCGTCGCCGGAAGTC AGACTGCTGCATGCGATATCGAGCTCTCCCGGG
ABH H3369A	CCCAAGCTTCTTCTAGAGGTACCGCATGCAATCACTACCAGAAGCAAGG TATCGATATGCTCGCAGTCAACCTGCGTGGCTATGGTGAAAGCGACGG TGGACCAAGCGAAAAAGGCTTGTACCAAGATGCTCGCACCATGTTCAAC TACCTAGTGAATGATAAGGGTATTGACCCAAGCAACATCATCATTCACG GCTACTCAATGGGCGGTCCAATTGCCGCAGATTTAGCACGTTATGCCG CGCAAAACGGCCAAGCGGTGTCTGGCTTATTGCTTGACCGTCCTATGC CAAGCATGACCAAAGCAATCACCGCTCACGAAGTGGCGAATCCAGCGG GCATTGTGGGGGCTATCGCGAAAGCGGTTAACGGCCAGTTCTCTGTAG AGAAAAATCTCGAAGGTTTGCCAAAAGAGACATCCATTCTGCTGTTGAC CGATAACGAAGGTTTGGGTAACGAAGGTGAGAAACTTCGTACCAAACTC ACTGCCTCTGGTTACAACGTCACTGGCGAGCAGACATTCTATGGT**GCT**G AAGCAAGCAACCGTTTGATGAGTCAATATGCGGATCAAATTGTCTCCGG TTTGTCCAGCAGTGCAAGTGTAGATGAAGACCTAGATCAACAAGGGTTG GATACCACATCAACCAAGGATCAAGGTATCTCAAATAAGAATGATCATCT GCAGGTGGTGGATAGTAAAGAAGCATTAGCGGATGGAAAAATACTCCAT AATCAAAATGTTAATAGCTGGGGCCCGATTACGGTTACACCAACGACAG ATGGTGGTGAAACCCGCTTCGACGGTCAAATCATCGTTCAAATGGAAAA CGACCCGGTAGTAGCAAAAGCGGCAGCCAATTTAGCAGGTAAACATGC TGAAAGCAGTGTGGTGGTGCAGCTCGATTCAGACGGCAACTATCGCGT GGTGTATGGCGATCCGTCAAAACTGGATGGAAAGCTACGTTGGCAGTT GGTGGGGCATGGTCGCGACCACTCAGAAACTAACAATACTCGCTTAAG TGGTTACAGTGCCGCATGCGATATCGAGCTCTCCCGGG

929 **Table S3 Primers used in study.**

Primer	Sequence	Function
IL-8_5'	AGCACTCCTTGGCAAAACTG	CXCL8 qPCR
IL-8_3'	CAAGAGCCAGGAAGAAACCA	CXCL8 qPCR
qTNF_5'	GCCAGAGGGCTGATTAGAGA	TNF qPCR
qTNF_3'	TCAGCCTCTTCTCCTTCCTG	TNF qPCR
qJUN_5'	GTCCTTCTTCTCTTGCGTGG	JUN qPCR
qJUN_3'	GGAGACAAGTGGCAGAGTCC	JUN qPCR
qFOS_5'	GGGGCAAGGTGGAACAGTTAT	FOS qPCR
qFOS_3'	CCGCTTGGAGTGTATCAGTCA	FOS qPCR
qCXCL3_5'	CGCCCAAACCGAAGTCATAG	CXCL3 qPCR
qCXCL3_3'	GCTCCCCTTGTTCAGTATCTTTT	CXCL3 qPCR
qEGR1_5'	AAAGCGGCCAGTATAGGTGA	EGR1 qPCR
qEGR1_3'	AGCCCTACGAGCACCTGAC	EGR1 qPCR
GAPDH_2_5' FWD	TTGAGGTCAATGAAGGGGTC	GAPDH qPCR
GAPDH_2_3' REV	GAAGGTGAAGGTCGGAGTCA	GAPDH qPCR
ACDVc_cat_FWD	GCACAAGCCGATGCTCAAGGTGCTAAACAAAAC	*acd* E1990A PCR
ACDVc_cat_REV	GTCTGACTTCCGGCGACGAGCTTGTACCAAATT	*acd* E1990A PCR
RIDVc_cat_FWD	GGCAAAGGTAATCTTGCCAATATCGATCTGCTAGG	*rid* H2782A PCR
RIDVc_cat_REV	CTCGATAAAGCGTTTCAGCTTAATGTCGCCATC	*rid* H2782A PCR
ABHVc_cat_FWD	CACTACCAGAAGCAAGGTATCGATATGTCGCAG	*abh* H3369A PCR
ABHVc_cat_REV	CCACTTAAGCGAGTATTGTTAGTTTCTGAG	*abh* H3369A PCR

930